Finite Element Modeling Of Retrofitted RC Beams

A thesis report submitted in the partial fulfillment of

requirement for the award of the degree of

MASTERS OF CIVIL ENGINEERING

IN

STRUCTURES

Submitted By

Himanshu Singhal

Roll No. 80722001

Under the supervision of

Dr. Naveen Kwatra

Associate Professor,

Civil Engg Deptt,

Thapar University, Patiala

Mrs. Shruti Sharma

Sr. Lecturer,

Civil Engg Deptt,

Thapar University, Patiala

DEPARTMENT OF CIVIL ENGINEERING

THAPAR UNIVERSITY,

PATIALA- 147004, (INDIA)

July-2009

CERTIFICATE

It is certified that the thesis report entitled **"Finite Element Modeling of Retrofitted RCC Beams"**, which is being submitted herewith by **Himanshu Singhal,** in partial fulfillment for the **award of degree in Master of Civil Engineering (Structures)** at **THAPAR UNIVERSITY, PATIALA** is an authentic record of student's own work carried out under my supervision and guidance. The matter presented in the thesis has reached the standards fulfilling the requirements of the regulation for the award of said degree.

Dr. Naveen Kwatra
Assistant Professor,
Civil Engg Deptt,
Thapar University, Patiala
(Supervisor)

Mrs. Shruti Sharma
Lecturer
Civil Engg Deptt.,
Thapar University, Patiala
(Supervisor)

Dr. Maneek Kumar
Head of Deptt,
Civil Engg Deptt
Thapar University, Patiala

Dr. R.K.Sharma
DOAA,
Thapar University, Patiala

ACKNOWLEDGEMENT

"SUCCESS BEGINS WITH A SINGLE STEPS"

A dissertation cannot be completed without the help of many peoples who contribute directly or indirectly through there constructive criticism in the evolution and preparation of this work. It would not be fair on my part, if I don't say a word of thanks to all those whose sincere advice made this period a real educative, enlightening, pleasurable and memorable one.

First of all, a special debt of gratitude is owned to my thesis supervisor, Associate Professor **Dr. Naveen Kwatra** and Lecturer **Mrs. Shruti Sharma** for their gracious efforts and keen pursuit, which has remained as a valuable asset for the successful instrument of my seminar report. His dynamism and diligent enthusiasm has been highly instrumental in keeping my spirit high. His flawless and forthright suggestions blended with an innate intelligent application have crowned my task a success.

My thanks are due to Dr. Maneek Kumar, Head of the Civil Engineering Department of this institute for providing excellent computational facilities and aid in preparation of the thesis.

My special thanks to Er. Jan Cervenka, Cervenka Consulting from Czech Republic for solving all the problems occurred in the software ATENA used in the thesis work. My work can't be completed without him as he replied me timely with the solutions of all the queries which I have been asked through e-mails.

I would also like to thank to my parents, brother and my friends for their constant encouragement during the entire course of my thesis work.

I am also like to offer my sincere thanks to all faculty, teaching and non-teaching of Civil Engineering Department (CED), and staff of central library, TU, Patiala for their assistance.

HIMANSHU SINGHAL

M.E CIVIL STRUCTURES

ROLL NO 80722001

ABSTRACT

Many structures damaged due to increasing load, earthquake and many other natural disasters, toxic emitted in the surrounding area and to rectify these structures, repair and rehabilitation has become an increasingly important challenge for the reinforced cement concrete structures. Upgrading structural load deformation capacity is a substantial part of the rehabilitation and retrofit of reinforced cement concrete components is now becoming a mainstream. As a combined result of structural rehabilitation needs, strengthening and retrofitting of concrete structural parts and now-a-days it becomes the major growth research area for the researchers. Amongst various methods developed for strengthening, the deflected parts of the structures and retrofitting of reinforced concrete (RC) beam structures, external bonding of fiber reinforced plastic (FRP) wrapping on to the beam has been widely accepted as an effective and convenient method. In particular, the flexural strength of a beam can be significantly increased by application of FRP sheets adhesively bonded to the beam tension face. The main advantages of FRP include high strength and stiffness, high resistance to corrosion, as well as light weight due to low density. The retrofitting can be applied economically, as there is no need for mechanical fixing and surface preparation. Moreover, the strengthening system with FRP can be easily maintained by finite element method.

The finite element method has thus become a powerful computational tool, which allows complex analyses of the nonlinear response of RC structures to be carried out in a routine fashion. With this method the importance and interaction of different nonlinear effects on the response of RC structures can be studied analytically.

The study deals with “Finite Element modeling of the Retrofitted RCC Beams” with the help of ATENA. The ATENA is new FEM based software which helps in FEM modeling the RCC structure. In this research, the first phase is to FE modeled the beams and analyze the results and also compare the results of stressed retrofitted beams with the control beam. The four simply supported half beams are modeled due to symmetry. Out of these beams, one beam was taken as control beam and other three beams were stressed at 60%, 75% and 90% of the ultimate load and after the stressing beams, they are retrofitted by using the GFRP sheet. Initially, the control beam was modeled in the ATENA and analyze. ATENA gave the load deflection curve, the ultimate

load and the ultimate deflection, stress strain values, cracking behavior at each steps etc. After getting the ultimate load and the ultimate deflection of the control beam, the other three beams are modeled one by one and stressed to their respective loads and then retrofitted modeling is done in ATENA. When all the stressed retrofitted beam are modeled, start analyze all three beams. All the results of the stressed retrofitted beams are collected and compare with the control beam results. The results showed that stressed retrofitted beam has higher ultimate load deflection than the control beam.

The second phase of this research is to compare the results with the experimental results and try to identify the various effects on the RCC structural members. The results show good agreement with the experimental results.

Only the control beam, analytical results showed some difference from the experimental results whereas the stressed retrofitted beam, analytical results show nearly the same results as experimental results.

TABLE OF CONTENTS

LIST OF FIGURES

LIST OF TABLES

Chapter 1

INTRODUCTION

1.1 General

Reinforced concrete (RC) structures get damaged due to various reasons. In most of the cases damage occurred in the form of cracks, concrete spalling, and large deflection, etc. There are various factors which are responsible for these deteriorations, such as increasing load, corrosion of steel, earthquake, environmental effects and accidental impacts on the structure. That's why repair and rehabilitation has become an increasingly important challenge for the reinforced cement concrete structures in recent years. It is necessary to that repair techniques should be suitable in terms of low costs and fast processing time. Externally bonded fibres reinforced polymers (FRP) has emerged as a new structural strengthening technology in response to the increasing need for repair and strengthening of reinforced concrete structures, because of their high tensile strength, lightweight, resistance to corrosion, high durability, and ease of installation. The FRP reinforcement has shown to be applicable to the strengthening of structural members or repairing of damaged structures of many types of RCC structures, such as columns, beams, slabs, etc. The FRP can be used to improve flexural and shear capacities, provide confinement and ductility to compression structural members. The FRP is characterized by high strength fibres embedded in polymer resin. The most common type of FRP in industry is made with carbon, aramid or glass fibres. Repairing RCC structures by externally bonded FRP composites consists in adhering FRP laminates at the tensile face of the beam. Among these types of FRP, the application of Glass fibre reinforced polymer (GFRP) to strengthen and repair the concrete beams has received the most attention from the research community. The major goals of the retrofitting are to strengthening the retrofitted structures for life safety and the protection of the structures. It is therefore, the existing deficient structures be retrofitted to improve their performance in the event of any natural disaster and to avoid large scale damage to life and property. Currently, FRP materials have been widely used to increase the flexural and shear capacity of RCC members. FRP sheet is advantageous over steel plate due to its low weight, high strength and non-corrosive property. In the light of above discussion, the only analytical tool which done the retrofitting modelling and able to calculate the non linear

behaviour of the structural members and also free from all the above flaws is Finite element method.

The finite element method has thus become a powerful computational tool, which allows complex analyses of the nonlinear response of RC structures to be carried out in a routine fashion. FEM helps in the investigation of the behaviour of the structure, before and after the loading conditions, its load deflection behaviour and the cracks pattern. Analytical research provides the basic information for finite element models, such as material properties. In addition, the results of finite element models have to be evaluated by comparing them with experiments of full-scale models of beams. The development of reliable analytical models can, however, reduce the number of required test specimens for the solution of a given problem; recognizing and conducting those tests are time-consuming and costly and often do not simulate exactly the loading and support conditions of the actual structure.

Many studied had done only on the retrofitted RC beams but no work can be done on the field of stressed retrofitted beam. Thats why, in this present study, deals with the finite element modelling and analysis of the Stressed Retrofitted beam at 60%, 75% and 90% of the ultimate load with GFRP. This study focuses on a finite element modelling to simulate the behaviour of RC beams retrofitted with GFRP.

1.2 Objectives

The present investigation of the nonlinear response to failure of RCC beams and the retrofitted RCC beams under the point loads is initiated with the intent to investigate the relative importance of several factors in the nonlinear finite element analysis of RCC beams: these include the variation in load displacement graph, the crack patterns, propagation of the cracks and the crack width and the effect of size of the finite element mesh on the analytical results and the effect of the nonlinear behaviour of concrete and steel on the response of control beam and the deformed beam.

The following are the main objectives of the present study:

1. To model the reinforced cement concrete beams called as a control beam and the stressed retrofitted reinforced cement concrete beams at 60%, 75% and 90% of the ultimate load of the control beam using FEM.

2. To determine analytically the load deflection curve of control beams and stressed retrofitted beam subject to 60%, 75% and 90%..
3. Compared the results of the control beam and the stressed retrofitted beam and also compared the analytical results with the experimental results.

1.3 Scope of the work

In the first phase of the present study to FEM modelling of the control RCC beam under the static point loads have been analyzed using ATENA software and the results so obtained have been compared to available experimental result from the work done by Goyal (2007). Firstly, FEM modelling of the half RCC beams due to the symmetry. The size of the beam is 4.1m X 0 .127m X 0.227m with a two point loads 1 m apart at the centre of the beam. The materials which used in a modelling are M 20 concrete and Fe 415 reinforced bars of diameter 10mm at the tension side, 8mm diameter bar at the compression side and for shear reinforced bar of 6mm diameter. The control beam is analyzed using ATENA software up to the failure and gets the load deformation curves and the cracking behaviour. The control beam has been analyzed and compared with the experimental results. In the second phase of the study, FEM modelling the stressed retrofitted RCC beams at 60%, 75% and 90% of the ultimate load of the control beam and analyzed. They are retrofitted by using GFRP. The analytical result of these beams compared with experimental results. Comparisons are made by the load deflection curves and values. Deflection and cracking behaviour of these RCC beams are also studied.

1.4 Outline of the Thesis

Following the introduction in Chapter 1, Chapter 2 discusses the literature review i.e. the experimental work done by various researchers in the same field. FEM modelling, theory related to the ATENA, material modelling and analytical programming procedure steps involved in modelling of the control beams and the retrofitted beams, some theory related to retrofitting of the RCC beams and GFRP also discussed in detailed in Chapter 3. It also deals with the description of the material behaviour of concrete, reinforced steel bars, epoxy and GFRP.The results which come out from the analysis, comparison between the analytical results and the experimental results, results comparison between the control beam and other stressed retrofitted beam and the cracking behaviour of the beams, all are discussed in Chapter 4. Finally, salient conclusion and recommendations of the present study is given in chapter 5.

Chapter 2

Literature Review

2.1 General

To provide a detailed review of the body of literature related to retrofitted reinforced cement concrete structures in its entirety would be too immense to address in this thesis. However, there are many good references that can be used as a starting point for research. This literature review and introduction will focus on recent contributions related to retrofitting techniques of the RCC structures, material used for retrofit and past efforts most closely related to the needs of the present work.

2.2 FE modelling and the Strengthening of RC Beams

Duthinh and Starnes, (2001) conducted an experiment on strengthening of reinforced concrete beams using carbon fibre reinforced polymer. The seven test beams were cast and strengthening externally with carbon fibre reinforced polymer (FRP) laminate after the concrete had cracked were tested under four-point bending. The results obtained from this experiment were that CFRP is very effective for flexural strengthening. As the amount of steel reinforcement increases, the additional strength provided by the carbon FRP external reinforcement decreases. The same FRP reinforcement more than doubled the strength of a lightly reinforced beam. Compared to a beam reinforced heavily with steel only, the beams reinforced with both steel and carbon have adequate deformation capacity, in spite of their brittle mode of failure. .

Yanga et.al, (2003) conducted an experiment on finite element modelling of concrete cover separation failure in FRP plated RC beams on the tension side of the reinforcement concrete beam. This paper deals with a fracture mechanics based finite element analysis of debonding failures. This study investigates the behaviour of an FRP plated RC beam using a discrete crack model based on FEA. Linear elastic fracture mechanics (LEFM) was used in this study and on-going research is being undertaken to extend this to use non-linear fracture mechanism. In this research, only half of the beam was modelled accounting for its symmetry. Four node quadrilateral isoparametric elements and three node constant strain elements were used to model the concrete, adhesive and CFRP plate. The internal steel reinforcements were modelled using two-node truss elements. The concrete was modelled by near square elements to simplify the

remeshing process. The concrete cover on the tension face was modelled using four layers of elements. Both the adhesive and the CFRP plate were modelled using one layer of elements. The results obtained from this study, in a preliminary study was successfully simulated the concrete cover separation failure mode in FRP strengthened RC beams. Initial numerical results confirmed that the bonding of a plate leads to smaller and more closely spaced cracks than the un-strengthened beam. For plated beams, the cracking can have a significant effect on the stress distribution in the FRP plates. The stress distribution is uniform in the constant bending moment span only before major cracks are developed or close to the ultimate state. The length of the plate has a significant effect on the failure mode. The numerical example showed that if all other parameters remain unchanged, a beam strengthened with a short plate is more likely to fail due to concrete cover separation and in a more brittle manner.

Perera and Recuero**, **(2004) studied the adherence analysis of fiber reinforced polymer strengthened RC beams. In this paper, discussed the effect of bonding between reinforced concrete and composite plates (CFRP) when epoxy adhesive is used. They compared the analytical and experimental results which came out from the works can be done in this paper. A test had been designed to characterize the behaviour of the adhesive connection between FRP and concrete; the test was based on the beam test, similar to the adherence test for steel reinforcement of concrete. In the same way, a numerical model based on finite elements has been developed to simulate the behaviour of RC members strengthened with FRP plates. The nonlinear response of the strengthened members is determined through the development of numerical material nonlinear constitutive models capable of simulating what happens experimentally. The results came out from this study was in the experimental tests, a local failure occurred mainly determined by high shear bond stresses transmitted to the concrete from the plates via adhesive. Debonding started at the mid span at the concrete blocks ends and propagated from there to the intermediate areas of the blocks. Therefore, it can be concluded that the shear bond stresses play a fundamental role in strengthening of RC beams with FRP plates. While in the analytical work, the model consider the position and increase of concrete cracks which has a very important influence on the overall response of the strengthened beam; it also affects the distribution of the stresses in the various locations of the member and the failure mechanism. In general, the model performs reasonably well in predicting the behaviour of the FRP strengthened beam.

Supaviriyakit et.al, (2004) performed analytically the non-linear finite element analysis of reinforced concrete beam strengthened with externally bonded FRP plates. The finite element modelling of FRP-strengthened beams is demonstrated in this paper. The key for success of the analysis is the correct material models of concrete, steel and FRP. The concrete and reinforcing steel are modelled together by 8-node 2-D isoparametric plane stress RC element. The RC element considers the effect of cracks and reinforcing steel as being smeared over the entire element. Concrete cracks and steel bars are treated in a smeared manner. The FRP plate is modelled by 2D elastic element. The epoxy layer can also be modelled by 2D elastic elements. Stress-strain properties of cracked concrete consist of tensile stress model normal to crack, compressive stress model parallel to crack and shear stress model tangential to crack. Stress strain property of reinforcement is assumed to be elastic-hardening to account for the bond between concrete and steel bars. FRP is modelled as elastic-brittle material. The objective of the test was to investigate the effect of the bonded length on peeling mode of FRP. The results obtained from this analytical work that the finite element analysis can accurately predict the load deformation, load capacity and failure mode of the beam. It can also capture cracking process for the shear-flexural peeling and end peeling failures, similar to the experiment.

Kumar and Chandranshekaran, (2004) performed the analysis of the retrofitted reinforced concrete shear beams using CFRP composites. This study presented the numerical study to simulate the behaviour of retrofitted reinforced concrete (RC) shear beams. The study was carried out on the control RC beam and retrofitted RC beams using carbon fibre reinforced plastic (CFRP) composites with ±45o and 90o fibre orientations. The effect of retrofitting on uncracked and precracked beams was studied too. The finite elements adopted by ANSYS were used in this study. The results obtained from this paper were the load deflection graph showed good agreement with the experimental plots. There was a difference in behaviour between the uncracked and precracked retrofitted beams though not significant. At ultimate stage there is a difference in behaviour between the uncracked and precracked retrofitted beams though not significant. This numerical modelling helps to track the crack formation and propagation especially in case of retrofitted beams in which the crack patterns cannot be seen by the experimental study due to wrapping of CFRP composites. This numerical study can be used to predict the behaviour of retrofitted reinforced concrete beams more precisely by assigning appropriate material properties. The crack patterns in the beams were also presented.

Ferracuti and Savoia, (2006) studied the numerical modelling for FRP-concrete delamination. A non-linear bond–slip model is presented for the study of delamination phenomenon. This research showed that FRP retrofit could be very useful to improve also the behaviour of the RC structure under both short term and long term service loadings. A non-linear interface law is adopted; the bonding between FRP plate and concrete is modelled by a non-linear interface law. A non-linear system of equations is then obtained via finite difference method. Newton–Raphson algorithm, different control parameters can be adopted in the various phases of delamination process (alternatively, force or displacements variables). Some numerical simulations are presented, concerning different delamination test setups and bond lengths. The numerical results of this study agree well with experimental data reported in the literature. A non-linear shear stress–slip law is adopted for the interface, which takes non-linear behaviour of concrete cover into account. Finite difference method is used to solve the non-linear system of governing equations. It is also shown that, adopting classical delamination test setup, snap-back behaviour in the load–displacement curve occurs for bonded plate lengths greater than the minimum anchorage length.

Bo Gao et.al *(2007)* deals with different failure mode of the FRP Strengthened RC beams i.e. (i) rupture of FRP strips; (ii) compression failure after yielding of steel; (iii) compression failure before yielding of steel; (iv) delamination of FRP strips due to crack; and (v) concrete cover separation. In this paper, a failure diagram is established to show the relationship and the transfer tendency among different failure modes for RC beams strengthened with FRP strips, and how failure modes change with FRP thickness and the distance from the end of FRP strips to the support. The results observed from this study after the comparison from many different literatures that epoxy bonding of fibre reinforced polymer (FRP) to the tension soffit of reinforced concrete (RC) beams can significantly improve the ultimate flexural strength and stiffness. The idea behind this failure diagram is that the failure mode associated with the lowest strain in FRP or concrete by comparison is most likely to occur. By comparison between predictions based on failure diagram and experimental results, we show that this method could predict the failure mode for a strengthened RC beam. Knowing the failure mode, the ultimate load capacity can be calculated. The failure diagram provides guidelines to practical design, and is useful in establishing a procedure for selecting the type and size of FRP for the external strengthening of RC beam.

Guido Camata et.al, (2007) presented a joint experimental–analytical investigation and studied the brittle failure modes of RCC members strengthened in flexure by FRP plates. Both mid span and plate end failure modes are studied. In the experimental work, four RC members were cast, two slabs and two beams. Out of these four members, one slab and one beam were tested as an unstrengthened member and the other one slab and one beam were tested as a strengthened member. Same work can be done analytically. These RC members were modelled and analyze through the finite element method. The FE model considers the actual crack pattern observed in the tests. The FEM uses both discrete and smeared crack discretization, because only a combination of the two crack model accurately traces the stiffness degradation of the strengthened members. The smeared crack mode was used for the beam concrete; the discrete crack model was used for the interfaces where delamination can be expected. The specimen was discretized using three-node triangular elements for the concrete matrix, the FRP and the resin. Line-to-line four-node interface elements were used for the interfaces and two-node truss elements for the steel reinforcement. The concrete continuum was modelled using a smeared crack model. The smeared crack model implemented in the program is based on a rotating crack concept, which allows the crack to align with the principal strain directions. The principles of the smeared crack model are that cracking occurs when the principal stress exceeds the tensile strength. Cracking is normal to the direction of the principal stress and the material softens in the post-peak regime. The strengthening of the RC beams was done with both CFRP and GFRP and notice the difference between these two materials. This paper shows how concrete cracking, adhesive behaviour, plate length, width and stiffness affect the failure mechanisms. The numerical and experimental work gave several results show that debonding and concrete cover splitting failure modes occur always by crack propagation inside the concrete. For short FRP plates, failure starts at the plates end, while the longer FRP plates, failure starts at mid span. A comparison between CFRP and GFRP strengthening with the same axial stiffness but different contact area showed that increasing the plate width increases greatly the peak load and the deformation level of the strengthened beam. The EB-FRP reinforcement width to RC member width ratio is important to determine whether the strengthened member fails due to either debonding or concrete cover splitting. The lower this ratio, the lower the probability of concrete covers splitting. The analyses also indicated that an important parameter is the distance between flexural and shear cracks.

N. Pannirselvam et.al (2008) done the experimental work for Strength Modelling of Reinforced Concrete Beam with Externally Bonded Fibre Reinforcement Polymer. In this study, three different steel ratios are used with two different Glass Fibre Reinforced Polymer (GFRP) types and two different thicknesses in each type of GFRP were used. 15 beams were casted for this work in which 3 were used as a control beam and the remaining were fixed with the GFRP laminate on the soffit. Flexural test, using simple beam with two-point loading was adopted to study the performance of FRP plated beams interms flexural strength, deflection, ductility and was compared with the unplated beams. The results obtained from this experiment showed that the beams strengthened with GFRP laminates exhibit better performance. The flexural strength and ductility increase with increase in thickness of GFRP plate. The increase in first crack loads was up to 88.89% for 3 mm thick Woven Rovings GFRP plates and 100.00% for 5 mm WRGFRP plated beams and increase in ductility in terms of energy and deflection was found to be 56.01 and 64.69% respectively with 5 mm thick GFRP plated beam. Strength models were developed for predicting the flexural strength (ultimate load, service load) and ductility of FRP beams.

M. Barbato et.al (2009) studied the efficient finite element modelling of reinforced concrete beams retrofitted with fibre reinforced polymers. This study presents a new simple and efficient two-dimensional frame finite element (FE) able to accurately estimate the load-carrying capacity of reinforced concrete (RC) beams flexurally strengthened with externally bonded fibre reinforced polymer (FRP) strips and plates. The proposed FE, denoted as FRP–FB beam, considers distributed plasticity with layer-discretization of the cross-sections in the context of a force-based (FB) formulation. The FRP–FB-beam element is able to model collapse due to concrete crushing, reinforcing steel yielding, FRP rupture and FRP debonding. The FRP–FB-beam is used to predict the load-carrying capacity and the applied load-mid span deflection response of RC beams subjected to three- and four-point bending loading. Numerical simulations and experimental measurements are compared based on numerous tests available in the literature and published by different authors. The numerically simulated responses agree remarkably well with the corresponding experimental results. The major features of this frame FE are its simplicity, computational efficiency and weak requirements in terms of FE mesh refinement. These useful features are obtained together with accuracy in the response simulation comparable to more complex, advanced and computationally expensive FEs. Thus, the FRP–FB-beam is

suitable for efficient and accurate modelling and analysis of flexural strengthening of RC frame structures with externally bonded FRP sheets/plates and for practical use in design-oriented parametric studies.

2.3 Gaps in Research Area

Many experimental and analytical works can be done from many researchers in the area of strengthening and retrofitting the structural members with composite materials. The concept of retrofitting the structural members is rapidly growing due to enable the early identification of damage and provides warning for unsafe condition. Some researchers have also investigated or work on the area of the failure mode of the FRP strengthened structural members and some are work on the strengthening of the structural members with different FRP materials.

This research is concerned with the finite element modelling of the retrofitted the RC beam using the GFRP. The use of GFRP sheets for retrofitting and the strengthening of the reinforced concrete structural have been studied extensively in previous studies. However, many researches performed experimentally analytically the strengthening of the beam but no works are to be done on field of stressed retrofitted structural members. That's why, with the help of ATENA, it is possible to model the stressed retrofitted beam and analyzed. ATENA also helps in FE modelling and meshing inside the beam of the surface. It gives the load deflection curve and gave the values of stress-strain, crack width of the beam and the material of the beam at every step which helps in modelling the deformed beam.

2.4 Direction for Present Research

The literature review suggested that use of a finite element modelling of the retrofitted reinforced cement concrete was indeed feasible. It was decided to use ATENA for the FE modelling. A reinforced concrete beam with reinforcing steel modelled discretely will be developed with results compared to the experimental work done by GOYAL (2007). The load-deflection curve of the experimental work will be compared to analytical predictions to calibrate the FE model for further use.

Chapter 3

FE Modelling of the Retrofitted RC Beam

3.1 Introduction

Over the last one or two decade numerical simulation of reinforced concrete structures and structural elements has become a major research area. A successful numerical simulation demands choosing suitable elements, formulating proper material models and selecting proper solution method.

This chapter discusses the theory related to ATENA and information about finite elements currently implemented in ATENA. All the necessary steps to create these models are explained in detail and the steps taken to generate the analytical load-deformation response of the joint are discussed.

With few exceptions all elements implemented in ATENA are constructed using isoparametric formulation with linear and/or quadratic interpolation functions. The isoparametric formulation of one, two and three dimensional elements belongs to the "classic" element formulations. This is not because of its superior properties, but due to the fact that it is a versatile and general approach with no hidden difficulties and, also very important, these elements are easy to understand. This is very important particularly in nonlinear analysis.

3.2 FINITE ELEMENT METHOD

The finite element method (FEM) or finite element analysis is a numerical technique for finding approximate solutions of partial differential equations (PDE) as well as of integral equations. The solution approach is based either on eliminating the differential equation completely (steady state problems), or rendering the PDE into an approximating system of ordinary differential equations, which are then numerically integrated using standard techniques.

In solving partial differential equations, the primary challenge is to create an equation that approximates the equation to be studied, but is numerically stable, meaning that errors in the input data and intermediate calculations do not accumulate and cause the resulting output to be

meaningless. The Finite Element Method is a good choice for solving partial differential equations over complex domains.

3.3 FINITE ELEMENT MODELING

The basic concept of FEM modelling is the subdivision of the mathematical model into disjoint (non-overlapping) components of simple geometry. The response of each element is expressed in terms of a finite number of degrees of freedom characterized as the value of an unknown function, or functions or at a set of nodal points. The response of the mathematical model is then considered to be the discrete model obtained by connecting or assembling the collection of all elements.

Within the framework of the finite element method reinforced concrete can be represented either by superimposition of the material models for the constituent parts (i.e., for concrete, for reinforcing steel and for FRP), or by a constitutive law for the composite concrete, embedded steel and composite FRP laminates considered as a continuum.

The finite element method is well suited for superimposition of the material models for the constituent parts of a composite material. Several constitutive models covering these effects are implemented in the computer code ATENA, which is a finite element package designed for computer simulation of concrete structures. The graphical user interface in ATENA provides an efficient and powerful environment for solving many anchoring problems. ATENA enables virtual testing of structures using computers, which is the present trend in the research and development world. Several practical examples of the utilization of ATENA for FEM stimulation of connections between steel and concrete. Material models of this type can be employed for virtually all kinds of reinforced concrete structural members.. Depending on the type of material modelling to be solved in ATENA, concrete can be represented by solid brick elements, the reinforcement is modelled by bar elements (discrete representation) and FRP is modelled by shell elements which can be described later.

Geometry and shape of any mathematical element helps in proper placement of the nodal points and materials properties helps in using proper modelling.

3.4. Material models

The program system ATENA offers a variety of material models for different materials and purposes. The most important material models in ATENA for RCC structure are concrete and reinforcement. These advanced models take into account all the important aspects of real material behaviour in tension and compression. In this study; the GFRP material modelling used for retrofitted RCC beams.

3.4.1 Concrete Modelling

1. Behaviour of the Concrete

Concrete exhibits a large number of microcracks, especially, at the interface between coarser aggregates and mortar, even before subjected to any load. The presence of these microcracks has a great effect on the mechanical behaviour of concrete, since their propagation during loading contributes to the nonlinear behaviour at low stress levels and causes volume expansion near failure. Many of these microcracks are caused by segregation, shrinkage or thermal expansion of the mortar. Some microcracks may develop during loading because of the difference in stiffness between aggregates and mortar. Since the aggregate-mortar interface has a significantly lower tensile strength than mortar, it constitutes the weakest link in the composite system. This is the primary reason for the low tensile strength of concrete.

The response of a structure under load depends to a large extent on the stress-strain relation of the constituent materials and the magnitude of stress. Since concrete is used mostly in compression, the stress-strain relation in compression is of primary interest.

2. Geometry of the Concrete

Element geometric modelling of concrete has been done using 3D solid brick element with 8 up to 20 nodes in ATENA, see fig 3.1

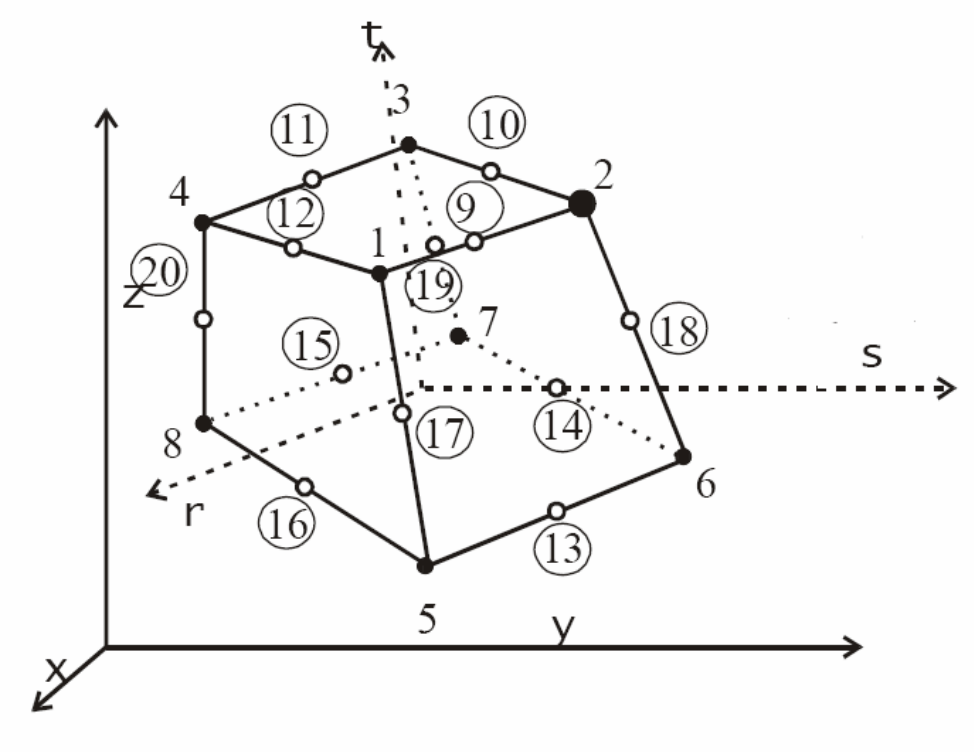

Fig. 3.1 Geometry of Brick elements

3. Element Properties

3D solid brick element having three degree of freedom at each node: translations in the nodal x, y and z directions. This is a iso parametric elements integrated by Gauss integration at integration points. This element is capable of plastic deformation, cracking in three orthogonal directions, and crushing. The most important aspect of this element is the treatment of nonlinear material properties.

4. Element Interpolation function

3D solid brick element interpolation functions for all variants of the elements are given below:

N_1= (1/8) (1+r) (1+s) (1+t)

N_2= (1/8) (1-r) (1+s) (1+t)

N_3= (1/8) (1-r) (1-s) (1+t)

N_4= (1/8) (1+r) (1-s) (1+t)

N_5= (1/8) (1+r) (1+s) (1-t)

N_6= (1/8) (1-r) (1+s) (1-t)

N_7= (1/8) (1-r) (1-s) (1-t)

N_8= (1/8) (1+r) (1-s) (1-t)

3.4.2 Reinforcement Modelling

1. Geometry of the reinforcement

Reinforcement modelling could be discrete or smeared. In our work, a discrete modelling of reinforcement has been done. The reinforcement has been modelled using bar elements in ATENA.

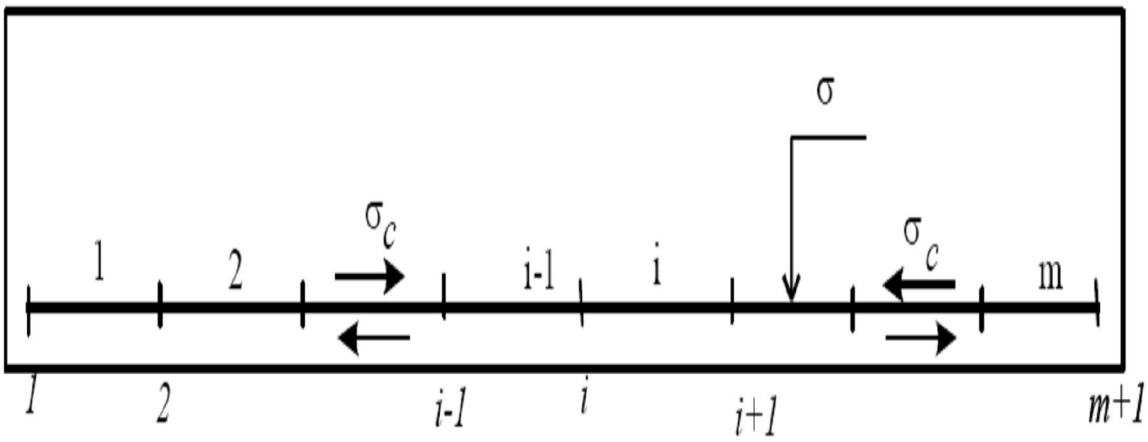

Fig 3.2 Geometry of the reinforcement

2. Element Properties

Reinforcement steel is a 3D bar element, which has three degrees of freedom at each node; translations in the nodal x, y and z direction. Bar element is a uniaxial tension-compression element. The stress is assumed to be uniform over the entire element. Also plasticity, creep, swelling, large deflection and stress-stiffening capabilities are included in the element.

3. Element Shape Functions:

The shape functions in natural co-ordinate system for the three dimensional bar element without rotational degrees of freedom.

$N_1 = (1/2)(1+s)$ $N_2 = (1/2)(1-s)$

3.4.3 FRP Modelling

The FRP modelling can be done as a 3D shell element in ATENA. The Ahmad shell element implemented in ATENA, described in ATENA theory manual. The present Ahmad element belongs to group of shell element formulation that is based on 3D elements concept. It can be used to model thin as well as thick shell or plate structures.

1. Geometry of the FRP

The FRP can be modelled as a shell element in ATENA. The Ahmad shell element used the 20 nodes isoparametric brick element as shown in fig. 3.3. This is needed, in order to be able to use the same pre and post-processors support for the shell and native 3D brick element. After the 1st step of the analysis, the input geometry will automatically change to the external geometry from fig. 3.3. As nodes 17 and 18 contain only so called bubble function, the element is post-processed in the same way is it would be the isoparametric brick element. Internally, all element's vectors and matrices are derived based on the internal geometry as depicted also shown in fig 3.3.

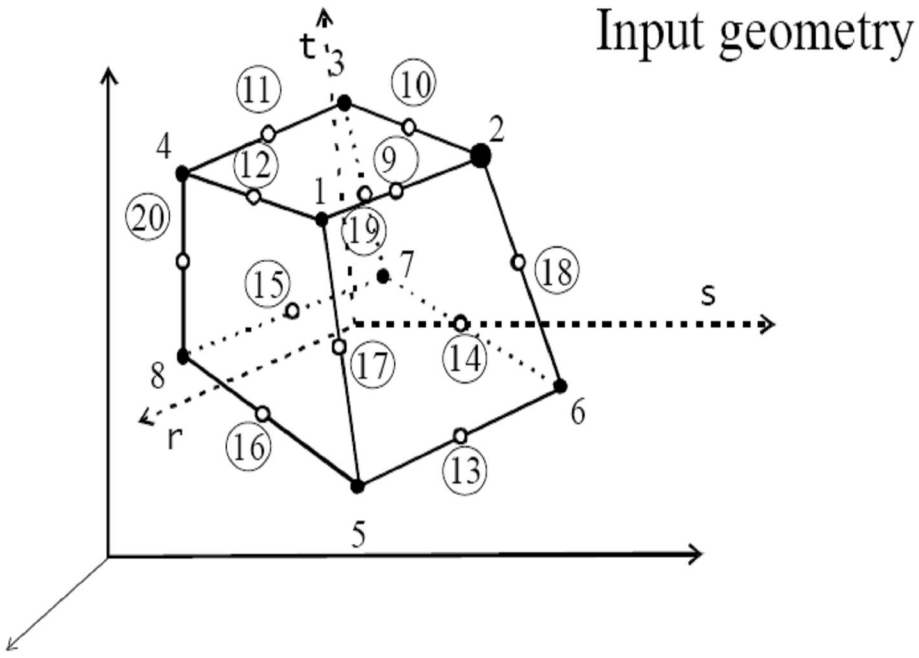

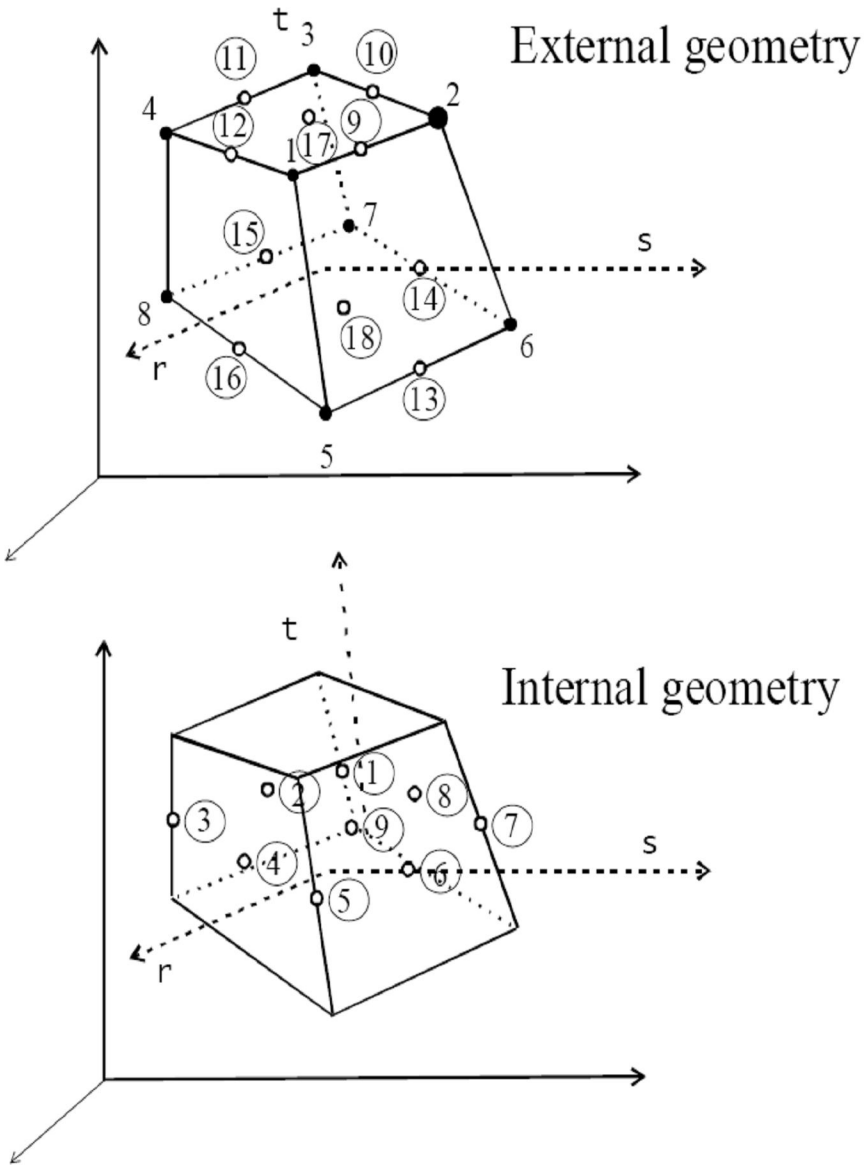

Figure 3.3 Geometry of the FRP

2. Element property of the FRP

FRP is a Ahmad shell element. In the following general shell element theory concept, every node of element has five degree of freedom, e.g. three displacements and two rotations in planes normal to mid surface of element. In order to facilitate a simple connection of this element with other true 3D elements, the (original) five degrees of freedom are transformed into x, y, z displacement of a top node and x, y displacement of a bottom node degrees of freedom. The two nodes are located on the normal to mid-surface passing thru the original mid-surface element's node.

3.5 *Stress-Strain Relations for Concrete*

3.5.1 Equivalent Uniaxial Law

The nonlinear behaviour of concrete in the biaxial stress state is described by means of the so called effective stress σ_c^{ef}, and the equivalent uniaxial strain ε^{eq}. The effective stress is in most cases a principal stress.

The equivalent uniaxial strain is introduced in order to eliminate the Poisson's effect in the plane stress state.

$$\boldsymbol{\varepsilon^{eq} = \sigma_{ci} / E_{ci}}$$

The equivalent uniaxial strain can be considered as the strain, that would be produced by the stress σ_{ci} in a uniaxial test with modulus associated E_{ci} with the direction *i*. Within this assumption, the nonlinearity representing damage is caused only by the governing stress σ_{ci}.

The complete equivalent uniaxial stress-strain diagram for concrete is shown in fig. 3.4.

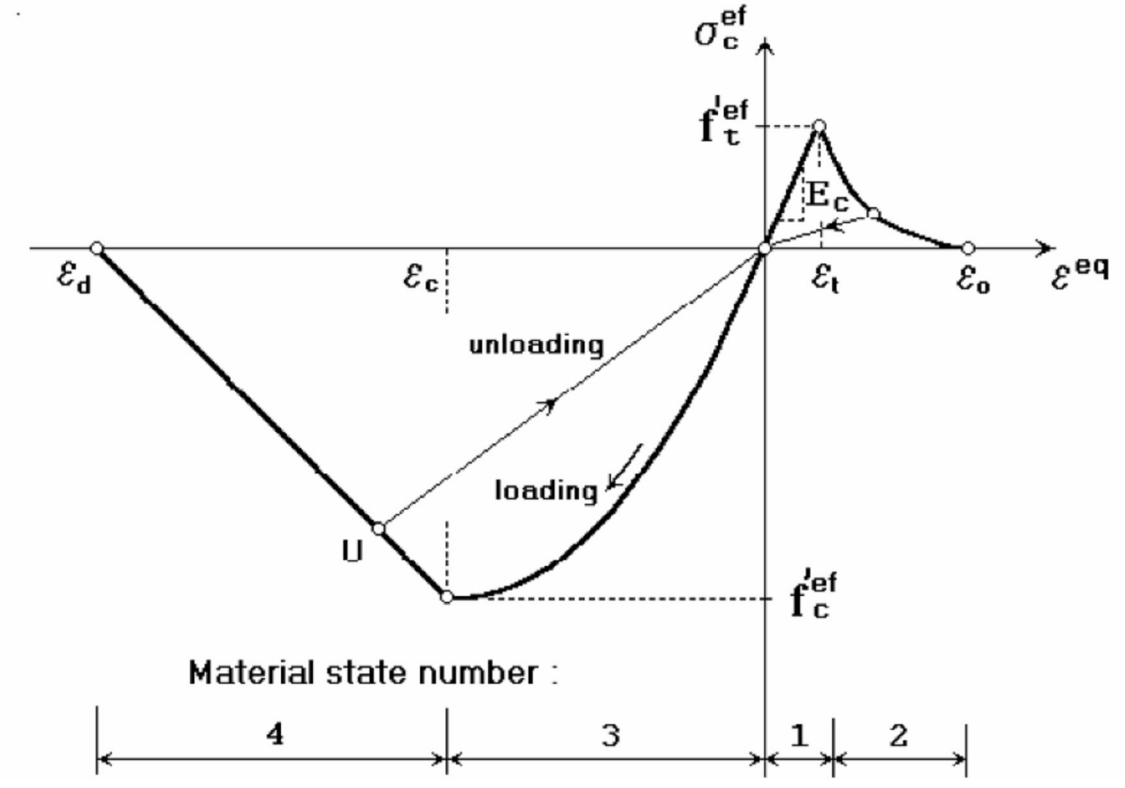

Fig. 3.4 Uniaxial stress-strain law for concrete.

The numbers of the diagram parts in fig. 3.4 (material state numbers) are used in the results of the analysis to indicate the state of damage of concrete.

Unloading is a linear function to the origin. An example of the unloading point *U* is shown in fig. 3.4. Thus, the relation between stress σ_c^{ef} and strain ε^{eq} is not unique and depends on a load history. A change from loading to unloading occurs, when the increment of the effective strain changes the sign. If subsequent reloading occurs the linear unloading path is followed until the last loading point *U* is reached again. Then, the loading function is resumed.

The peak values of stress in compression f'^{ef}_c and in tension f'^{ef}_t are calculated according to the biaxial stress state. Thus, the equivalent uniaxial stress-strain law reflects the biaxial stress state.

Biaxial Stress Failure Criterion of Concrete

1 Compressive Failure

A biaxial stress failure criterion according to KUPFER et al. (1969) is used as shown in fig. 3.5. In the compression-compression stress state the failure function is

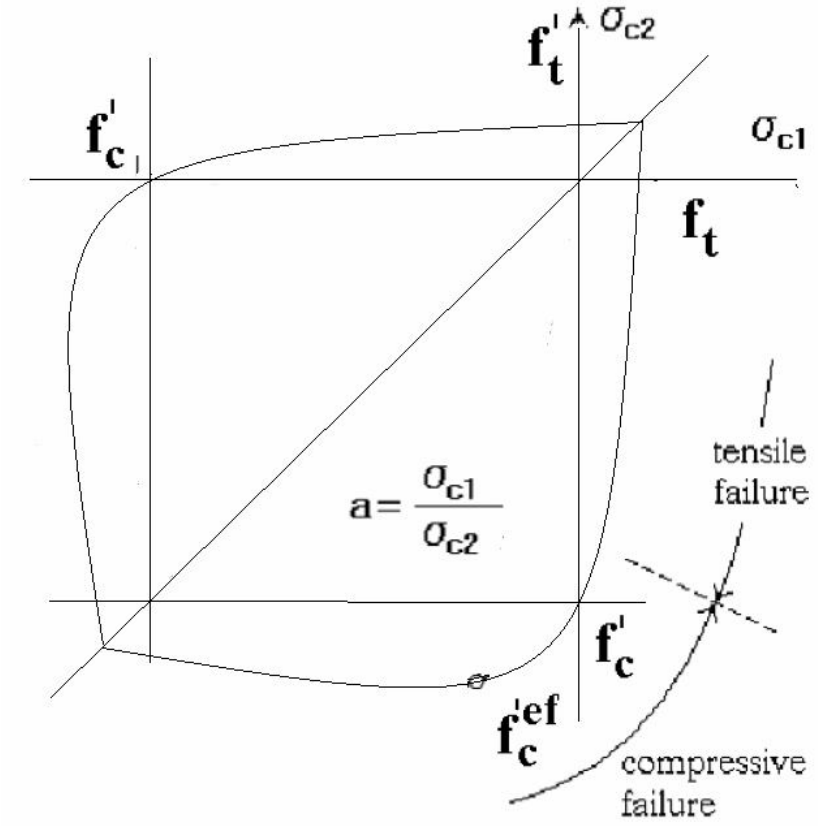

Fig. 3.5 Biaxial failure functions for concrete.

$$\mathbf{f'_c{}^{ef} = [(1+3.65a)/(1+a)^2]f'_c;\quad a = (\sigma_{c1}/\sigma_{c2})} \qquad (3.1)$$

where $\sigma_{c1,}\ \sigma_{c2}$ are the principal stresses in concrete and f'_c is the uniaxial cylinder strength. In the biaxial stress state, the strength of concrete is predicted under the assumption of a proportional stress path.

In the tension-compression state, the failure function continues linearly from the point $\sigma_{c1} = 0$, $\sigma_{c2} = f'_{c,}$ into the tension-compression region with the linearly decreasing strength:

$$\mathbf{f'_c{}^{ef} = f'_c\, r_{ec},\qquad r_{ec} = [1+ 5.3278(\sigma_{c1}/\, f'_c)]} \qquad (3.2)$$

where r_{ec} is the reduction factor of the compressive strength in the principal direction 2 due to the tensile stress in the principal direction 1.

2 Tensile failures

In the tension-tension state, the tensile strength is constant and equal to the uniaxial tensile strength f'_t. In the tension-compression state, the tensile strength is reduced by the relation:

$$\mathbf{f'^{ef}_t = f'_t\ r_{et}} \qquad (3.3)$$

where r_{et} is the reduction factor of the tensile strength in the direction 1 due to the compressive stress in the direction 2. The reduction function has one of the following forms, fig. 3.6.

$$\mathbf{r_{et} = 1 - 0.8\ (\sigma_{c2}/\, f'_c)} \qquad (3.4)$$

$$\mathbf{r_{et} = [A + (A - 1)\, B]/\, AB;\ B = Kx + A;\ x = \sigma_{c2}/\, f'_c} \qquad (3.5)$$

The relation in Eq. (3.4) is the linear decrease of the tensile strength and (3.5) is the hyperbolic decrease.

Two predefined shapes of the hyperbola are given by the position of an intermediate point *r, x.* Constants *K* and *A* define the shape of the hyperbola. The values of the constants for the two positions of the intermediate point are given in the following table.

Type	*Point*		*Parameters*	
	r	**X**	**A**	**K**
A	0.5	0.4	0.75	1.125
B	0.5	0.2	1.0625	6.0208

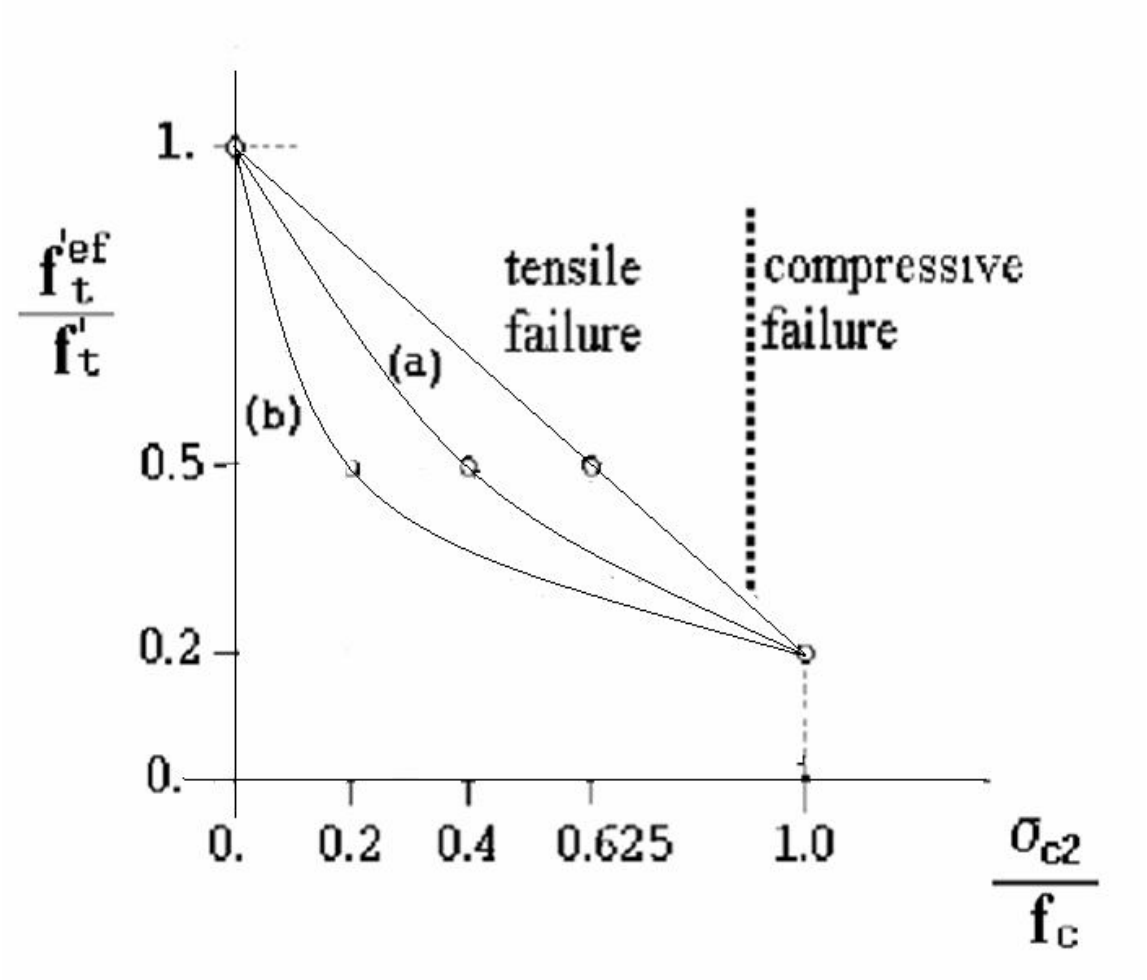

Figure 3.6 Tension-compression failure functions for concrete.

3.5.2 Tension before Cracking

The behaviour of concrete in tension without cracks is assumed linear elastic. E_c is the initial elastic modulus of concrete, f'^{ef}_t is the effective tensile strength derived from the biaxial failure function already describe above.

$$\sigma_c^{ef} = E_c\, \varepsilon^{eq},\ 0 < \sigma_c < f'^{ef}_t$$

3.5.3 Tension after Cracking

A fictitious crack model based on a crack-opening law and fracture energy. This formulation is suitable for modelling of crack propagation in concrete. It is used in combination with the crack band.It is a region (band) of material, which represents a discrete failure plane in the finite element analysis. In tension it is a crack, in compression it is a plane of crushing. In reality these failure regions have some dimension. However, since according to the experiments, the dimensions of the failure regions are independent on the structural size, they are assumed as fictitious planes. In case of tensile cracks, this approach is known as rack the "crack band theory", BAZANT, OH (1983). Here is the same concept used also for the compression failure. The purpose of the failure band is to eliminate two deficiencies, which occur in connection with the application of the finite element model: element size effect and element orientation effect.

1. Element size effect.

The direction of the failure planes is assumed to be normal to the principal stresses in tension and compression, respectively. The failure bands (for tension L_t and for compression L_c) are defined as projections of the finite element dimensions on the failure planes as shown in Fig. 3.7.

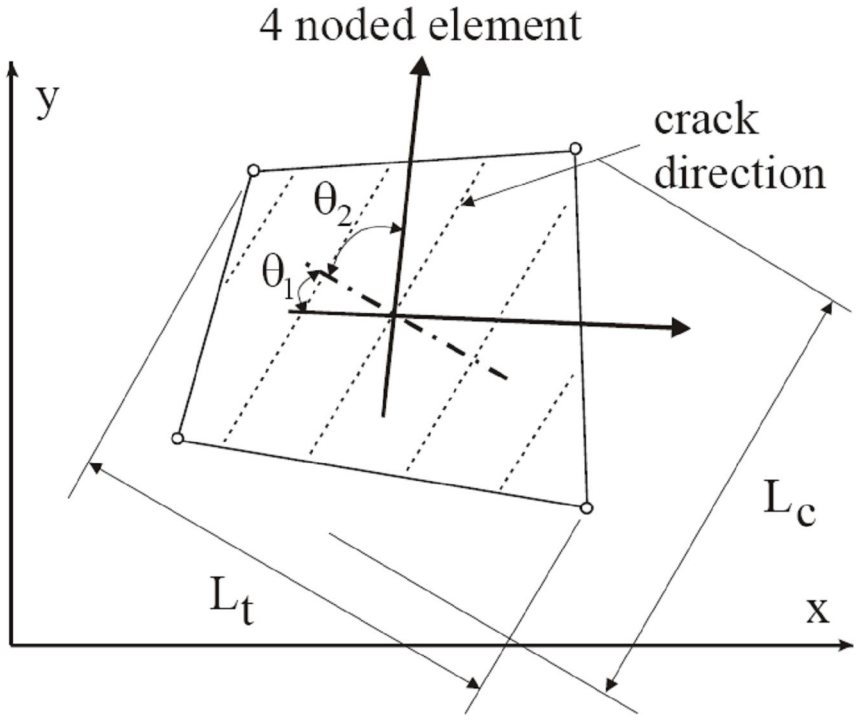

Figure 3.7 Definition of localization bands.

2 Element Orientation Effect.

The element orientation effect is reduced, by further increasing of the failure band for skew meshes, by the following formula (proposed by CERVENKA et al. 1995).

$$\mathbf{L_t = \gamma L_t,\ L_c = \gamma L_c}$$

$$\gamma = 1 + (\gamma^{max} - 1)\ (\theta / 45), \qquad \theta\ \varepsilon\ (0; 45) \qquad (3.6)$$

An angle θ is the minimal angle (min (θ_1, θ_2)) between the direction of the normal to the failure plane and element sides. In case of a general quadrilateral element the element sides' directions are calculated as average side directions for the two opposite edges. The above formula is a linear interpolation between the factor γ=1.0 for the direction parallel with element sides, and $\gamma=\gamma^{max}$, for the direction inclined at 45o. The recommended (and default) value of γ max =1.5.

3.6 Behaviour of Cracked Concrete

3.6.1 Description of a Cracked Section

The nonlinear response of concrete is often dominated by progressive cracking which results in localized failure. The structural member has cracked at discrete locations where the concrete tensile strength is exceeded.

At the cracked section all tension is carried by the steel reinforcement. Tensile stresses are, however, present in the concrete between the cracks, since some tension is transferred from steel to concrete through bond. The magnitude and distribution of bond stresses between the cracks determines the distribution of tensile stresses in the concrete and the reinforcing steel between the cracks.

Additional cracks can form between the initial cracks, if the tensile stress exceeds the concrete tensile strength between previously formed cracks. The final cracking state is reached when a tensile force of sufficient magnitude to form an additional crack between two existing cracks can no longer be transferred by bond from steel to concrete.

As the concrete reaches its tensile strength, primary cracks form. The number and the extent of cracks are controlled by the size and placement of the reinforcing steel. At the primary cracks the concrete stress drops to zero and the steel carries the entire tensile force. The concrete between

the cracks, however, still carries some tensile stress, which decreases with increasing load magnitude. This drop in concrete tensile stress with increasing load is associated with the breakdown of bond between reinforcing steel and concrete. At this stage a secondary system of internal cracks, called bond cracks, develops around the reinforcing steel, which begins to slip relative to the surrounding concrete.

Since cracking is the major source of material nonlinearity in the serviceability range of reinforced concrete structures, realistic cracking models need to be developed in order to accurately predict the load-deformation behaviour of reinforced concrete members. The selection of a cracking model depends on the purpose of the finite element analysis. If overall load-deflection behaviour is of primary interest, without much concern for crack patterns and estimation of local stresses, the "smeared" crack model is probably the best choice. If detailed local behaviour is of interest, the adoption of a "discrete" crack model might be necessary. Unless special connecting elements and double nodes are introduced in the finite element discretization of the structure, the well established smeared crack model results in perfect bond between steel and concrete, because of the inherent continuity of the displacement field.

3.6.2. Modelling of Cracking in Concrete

The need for a crack model that offers automatic generation of cracks and complete generality in crack orientation, without the need of redefining the finite element topology

The process of crack formation can be divided into three stages, Fig. 3.8. The uncracked stage is before a tensile strength is reached. The crack formation takes place in the process zone of a potential crack with decreasing tensile stress on a crack face due to a bridging effect. Finally, after a complete release of the stress, the crack opening continues without the stress.

The tension failure of concrete is characterized by a gradual growth of cracks, which join together and eventually disconnect larger parts of the structure. It is usually assumed that cracking formation is a brittle process and that the strength in tension loading direction abruptly goes to zero after such cracks have formed.

Therefore, the formation of cracks is undoubtedly one of the most important nonlinear phenomenons, which governs the behaviour of the concrete structures. In the finite element analysis of concrete structures, two principally different approaches have been employed for crack modelling. These are (a) discrete crack modelling (b) smeared crack modelling

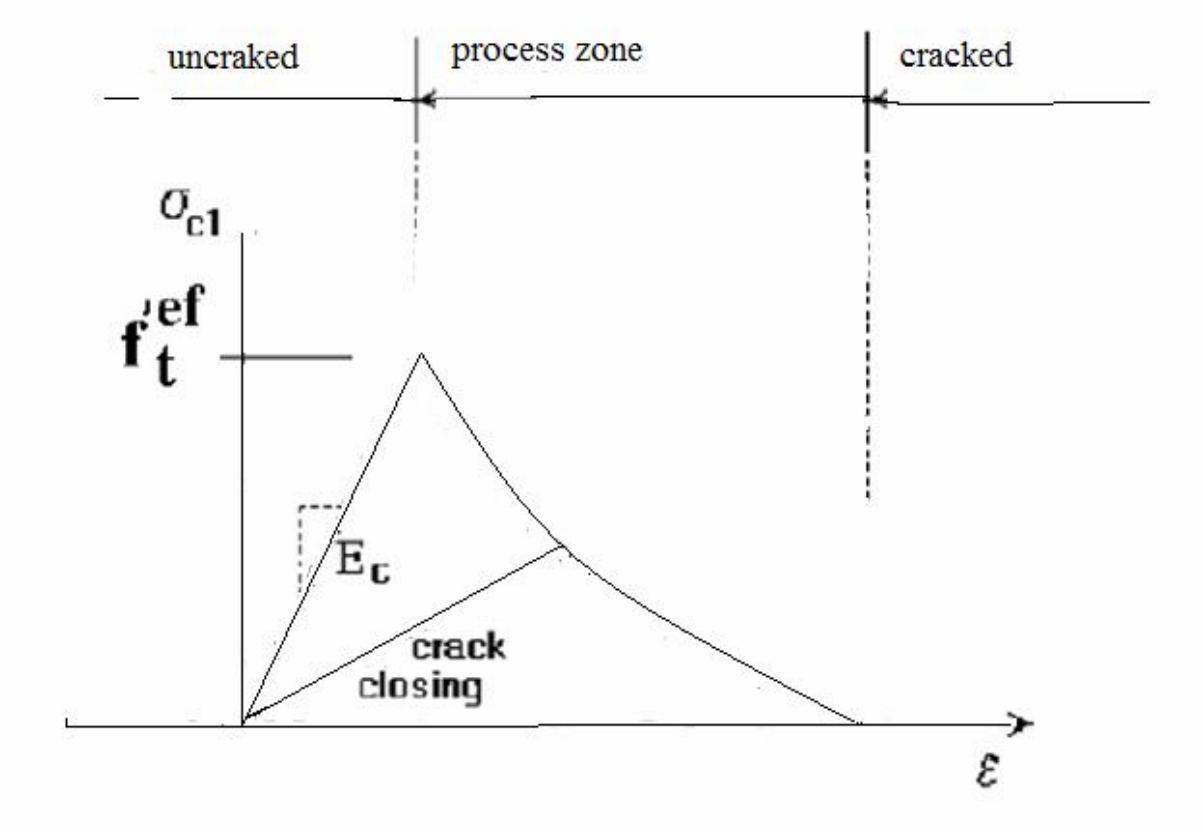

Figure3.8 Stages of Cracking Opening

.

The discrete approach is physically attractive but this approach suffers from few drawbacks, such as**,** it employs a continuous change in nodal connectivity, which does not fit in the nature of finite element displacement method; the crack is considered to follow a predefined path along the element edges and excessive computational efforts are required.

The second approach is the smeared crack approach. In this approach the cracks are assumed to be smeared out in a continuous fashion. Within the smeared concept two options are available for crack models: the fixed crack model and the rotated crack model. In both models the crack is formed when the principal stress exceeds the tensile strength. It is assumed that the cracks are uniformly distributed within the material volume. This is reflected in the constitutive model by an introduction of orthotropy.

1. Fixed Crack Model

In the fixed crack model (CERVENKA 1985, DARWIN 1974) the crack direction is given by the principal stress direction at the moment of the crack initiation. During further loading this direction is fixed and represents the material axis of the orthotropy.

The principal stress and strain directions coincide in the uncracked concrete, because of the assumption of isotropy in the concrete component. After cracking the orthotropy is introduced. The weak material axis m_1 is normal to the crack direction; the strong axis *m2* is parallel with the cracks.

In a general case the principal strain axes ε_1 and ε_2 rotate and need not to coincide with the axes of the orthotropy *m1* and *m2*. This produces a shear stress on the crack face as shown in Fig. 3.9. The stress components σ_{c1} and $\sigma c2$ denote, respectively, the stresses normal and parallel to the crack plane and, due to shear stress, they are not the principal stresses.

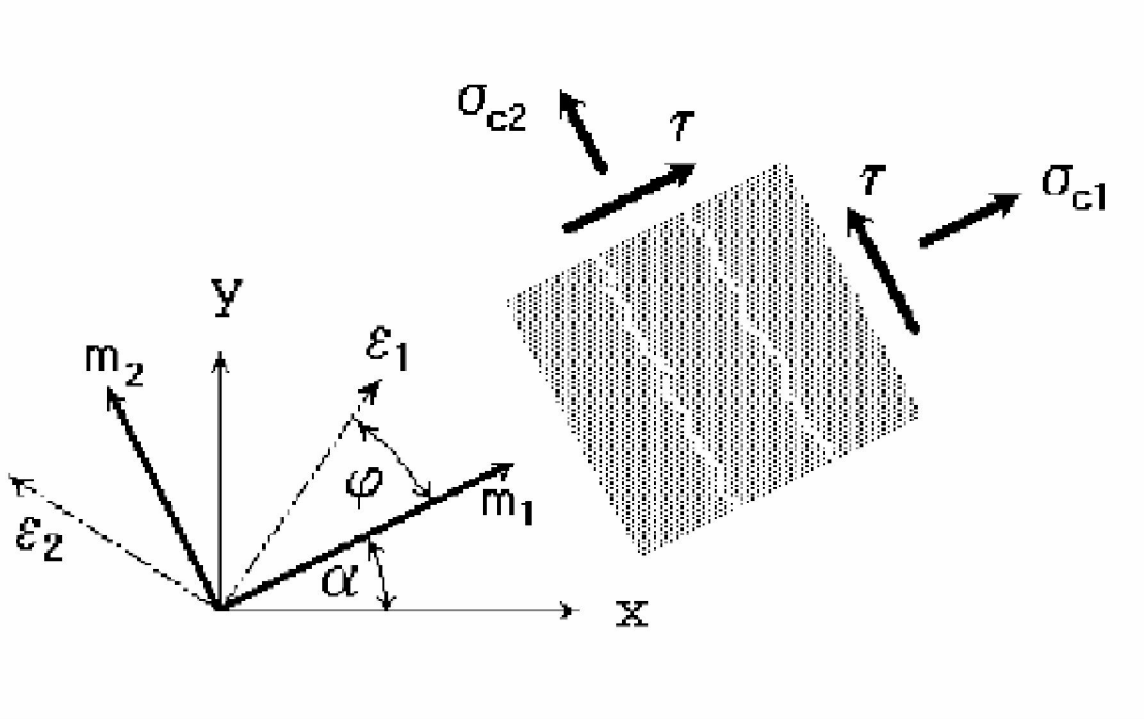

Figure 3.9 Fixed crack model. Stress and strain state.

2 Rotated Crack Model

In the rotated crack model (VECCHIO 1986, CRISFIELD 1989), the direction of the principal stress coincides with the direction of the principal strain. Thus, no shear strain occurs on the crack plane and only two normal stress components must be defined, as shown in Fig. 3.10.

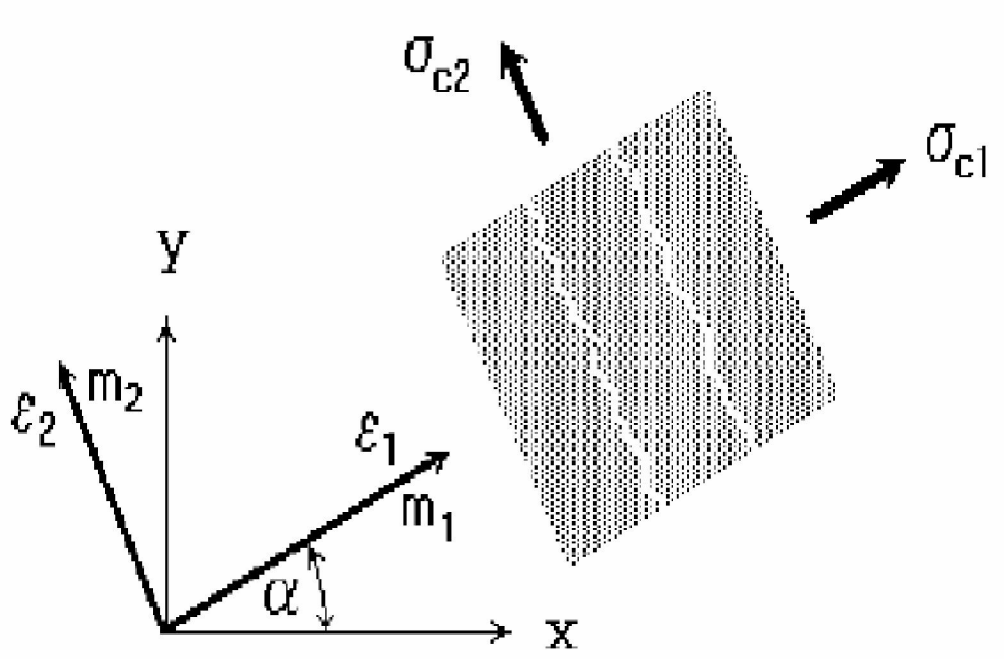

Fig. 3.10 Rotated crack model. Stress and strain state.

If the principal strain axes rotate during the loading the direction of the cracks rotates, too. In order to ensure the co-axiality of the principal strain axes with the material axes the tangent shear modulus *Gt* is calculated according to CRISFIELD 1989 as

$$G_t = (\sigma_{c1} - \sigma_{c2}) / 2\,(\varepsilon_1 - \varepsilon_2)$$

3.7 Stress-Strain Laws for Reinforcement

3.7.1 Introduction

Reinforcement can be modelled in two distinct forms: discrete and smeared. Discrete reinforcement is in form of reinforcing bars and is modelled by truss elements. The smeared

reinforcement is a component of composite material and can be considered either as a single (only one-constituent) material in the element under consideration or as one of the more such constituents. The former case can be a special mesh element (layer), while the later can be an element with concrete containing one or more reinforcements. In both cases the state of uniaxial stress is assumed and the same formulation of stress-strain law is used in all types of reinforcement.

3.7.2 Bilinear Law

The bilinear law, elastic-perfectly plastic, is assumed as shown in fig. 3.11

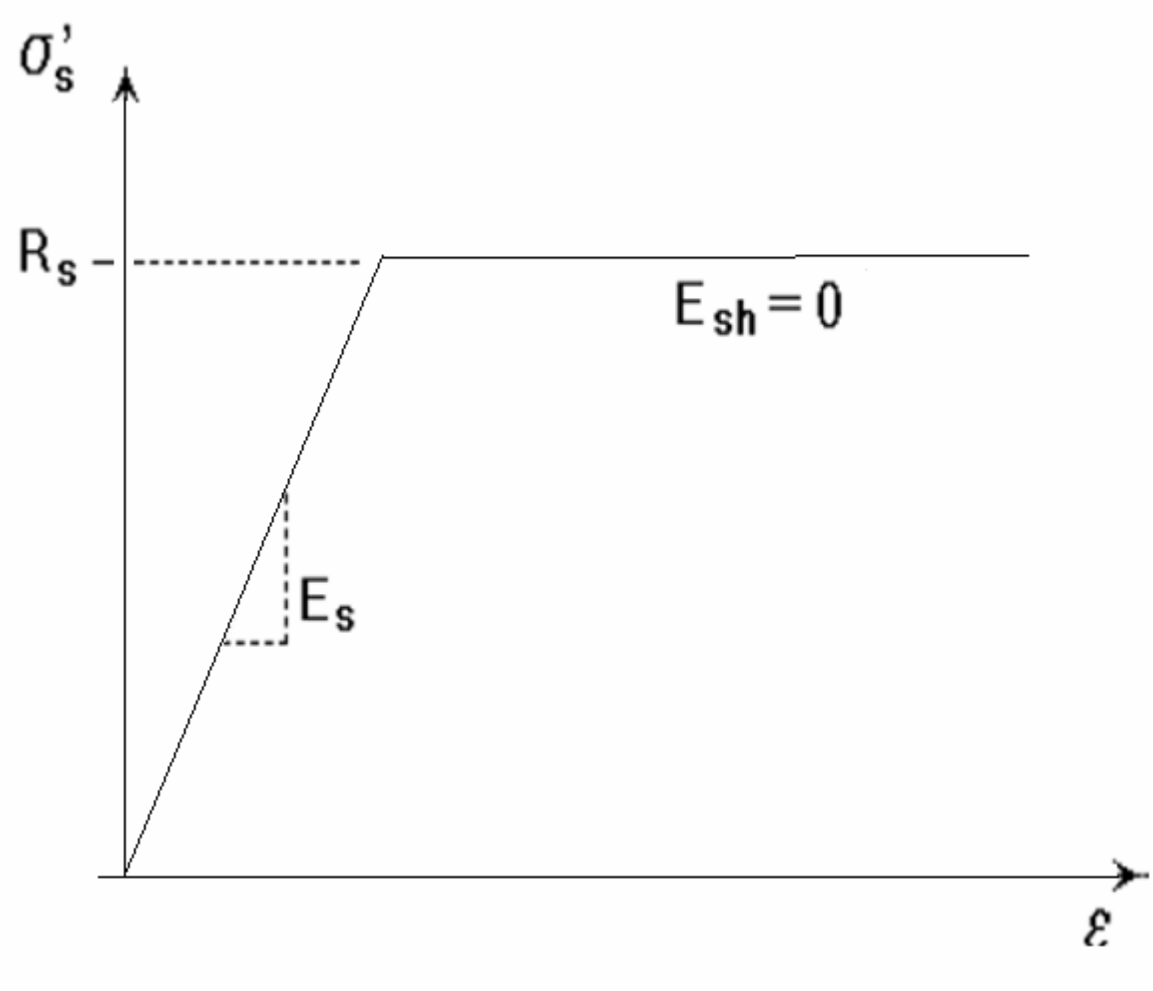

Figure 3.11 The bilinear stress-strain law for reinforcement.

The initial elastic part has the elastic modulus of steel E_s. The second line represents the plasticity of the steel with hardening and its slope is the hardening modulus E_{sh}. In case of perfect plasticity E_{sh} =0. Limit strain ε_L represents limited ductility of steel.

3.7.3 Multilinear Law

The multi-linear law consists of four lines as shown in fig. 3.12. This law allows to model all four stages of steel behaviour: elastic state, yield plateau, hardening and fracture. The multi-line is defined by four points, which can be specified by input.

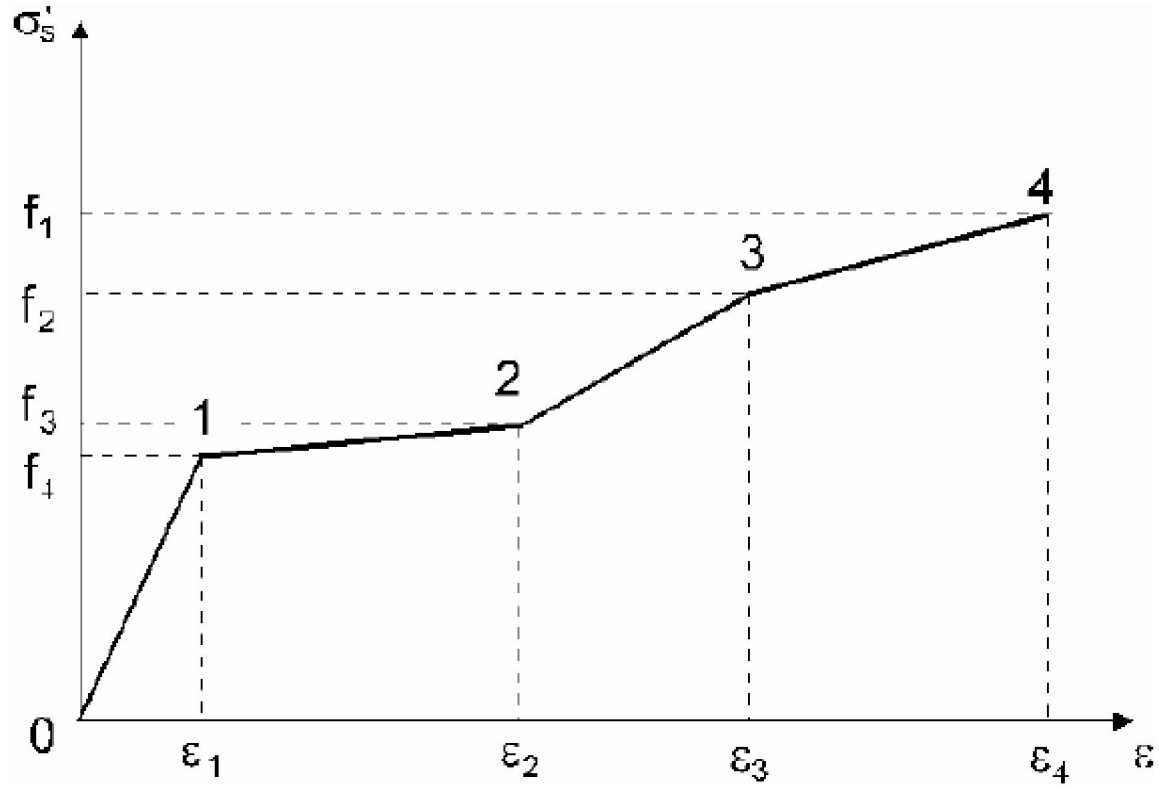

Fig. 3.12 The multi-linear stress-strain law for reinforcement.

The above described stress-strain laws can be used for the discrete as well as the smeared reinforcement. The smeared reinforcement requires two additional parameters: the reinforcing ratio p and the direction angle β as shown in fig. 3.13.

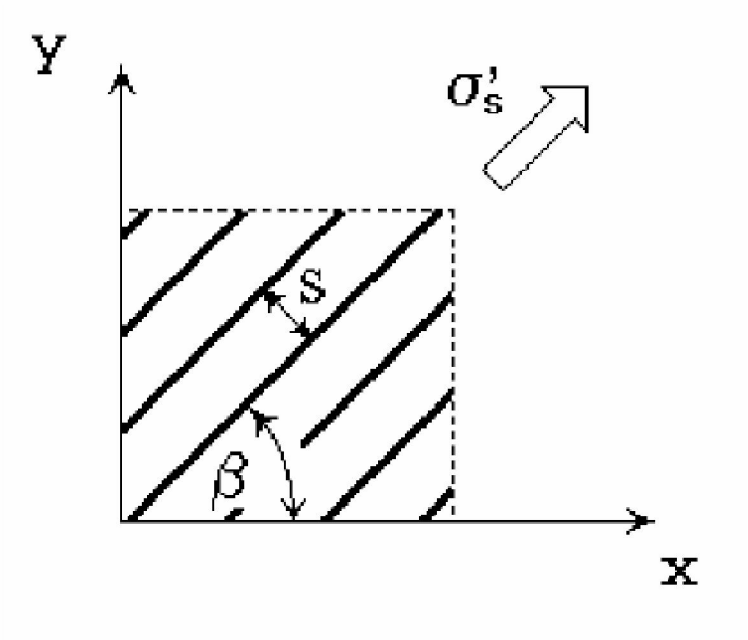

Figure 3.13 Smeared reinforcement.

Where ρ = (Area of steel/ Area of concrete)

The spacing *s* of the smeared reinforcement is assumed infinitely small. The stress in the smeared reinforcement is evaluated in the cracks, therefore it should include also a part of stress due to tension stiffening.

$$\sigma_{scr} = \sigma_s + \sigma_{ts}$$

where σ_s is the steel stress between the cracks (the steel stress in smeared reinforcement),

σ_{scr} is the steel stress in a crack. If no tension stiffening is specified $\sigma_{ts} = 0$ and $\sigma_{scr} = \sigma_s$. In case of the discrete reinforcement the steel stress is always σ_s.

Once we understand the finite element modelling, the next step is the analytical programming. The main objective of this analytical program is to get the result of under reinforced concrete beam and compare with the experimental results. In the analytical programming, first we select the materials and its properties and create geometry of the beams. For this, four beams are created and done the FE modelling through automatic FE mesh generator in ATENA. Out of these beams, one beam was taken as a control beam and the remaining three beams were taken as stressed retrofitted beams to 60%, 75%, and 90%. All these beams were tested up to its failure point and find out the ultimate load deflection values and in between graphs. For modelling the

control and retrofitted beams in ATENA, concrete, reinforcement bars of different diameters, steel plates, epoxy and GFRP is used a material.

3.8 Material Properties

Concrete, reinforcement steel, steel plates, Epoxy and GFRP used to model the RCC beam. The specification and the properties of these materials are as under:

1. Concrete

In ATENA, concrete material is taken as a 3D nonlinear cementitious2. The physical properties required for this material are given in table 3.1. Some properties of the concrete are taken from the Goyal (2007) thesis reports, some are the calculated values as per IS code 456:2000 and remaining are the default values.

Table 3.1 Material Properties of Concrete

Properties	Values
Elastic Modulus (Fresh concrete)	26692.7 MPa
Elastic Modulus (60% stressed concrete)	1811 MPa
Elastic Modulus (75% stressed concrete)	1471 MPa
Elastic Modulus (90% stressed concrete)	935 MPa
Poisson Ratio	0.2
Tensile Strength	3.737 MPa
Compressive Strength	28.5 MPa
Specific Fracture Energy	4.421E-05 MN/m
Critical Compressive Displacement	5E-04
Plastic Strain at Compressive Strength	6.681E-04
Reduction of Compressive Strength	0.8
Fail Surface Excentricity	0.52
Multiplier for the Plastic flow direction	0
Specific Material weight	0.024 MN/mE+3
Coefficient of Thermal Expansion	1E-05 1/K
Fixed Crack Model Coefficient	1

2. Reinforcement Bars

HYSD steel of grade Fe-415 of 10mm, 8mm and 6mm diameter were used as longitudinal steel. 10mm diameter bars are used as tension reinforcement and 8mm diameter bars are used as compression steel and 6mm diameter bars are used as shear reinforcement. The properties of these bars are shown in table 3.2.

Table 3.2 Material Properties of Reinforcement

Properties		Values
Elastic modulus		200000 MPa
Yield Strength	10mm diameter bar	445.55 MPa
	8 mm diameter bar	559.50 MPa
	6 mm diameter bar	442.42 MPa
Specific Material weight		.0785 MN/mE+3
Coefficient of Thermal Expansion		1.2E-05 1/K

3. Steel Plate

The function of the steel plate in the ATENA is for support and for loading. Here, the property of steel plate is same as the reinforcement bar except its yield strength. The HYSD steel of grade Fe-415 was used for steel plate.

4. Epoxy

Mbrace saturant was used as a epoxy in the analysis. The material properties are taken from the "Watson Bowman Acme corp." company paper. The material properties of epoxy are shown in table 3.3.

Table 3.3 Material Properties of Epoxy

Properties	Values
Elastic Modulus	3035 MPa
Poisson Ratio	0.4
Yield Strength	54 MPa
Hardening Modulus	0 MPa
Specific Material Weight	0.00983 MN/mE+3
Coefficient of Thermal Expansion	5.75E-05 1/K

5. Glass Fibre Reinforcement Polymer

Mbrace G sheet EU-900 unidirectional Glass fibre sheet is used in retrofitting. The properties which are used in the modelling are taken from the Mbrace Product Data, shown in the table 3.4.

Table 3.4 Material Properties of GFRP

Properties	Values
Strain, stress	(0,0); (0.005,390); (0.01,690) MPa
Specific Material Weight	0.026 MN/mE+3
Coefficient of Thermal Expansion	5.E-06 1/K

3.9 FE Modelling of RCC Beam in ATENA

According to the design, the dimension of the beam was 4.1 m length, 0.127 m breadth and 0.227 m depth. Due to the symmetric of the shape of the beam and the loading pattern, half beam was model. The reasons behind modelling the half beam were ease of calculation, lesser time consumption at the time of analysis, and easy for creating the geometry.

Four beams were modelled in ATENA. One is the control beam and the remaining three beams were stressed retrofitted beams with a use of GFRP at 60%, 75% and 90% of the ultimate load of the control beam.

Firstly non linear FE modelling of the control beam was done in ATENA and analyzes it to get the results. From the help of control beam results, other three beams were modelled and analyze it. All the results discussed in chapter 4.

In Atena, a very simple procedure has been given for modelling the RCC structure. ATENA has divide into three parts: Pre-processing, Run and Post-processing. The Pre-processing explains the basic steps, which are to be performed in order to define a complete geometry of the structural parts or structure, and then a finite element model for non-linear FE analysis by ATENA. The purpose of the geometrical model is to describe the geometry of the structure, its material properties and boundary conditions. The analytical models for the finite element analysis are created during the pre-processing with the help of the fully automated mesh generator. The geometrical model is composed of three-dimensional solid regions called “macro-elements”.

Hence in Atena, firstly define the material groups and material properties which are required by selecting the item **Materials** from the data access tree. After defining all the material properties, create geometry of the beam by selecting Macro element and define also the material property of the created geometry of the beam. The beam was modelled using three dimensional solid elements for concrete and embedded linear truss elements for steel. This structural element was selected according to the experimental evidence. Once the geometry model of the beam created proceeds to the next step i.e the FE numerical model. The FE numerical model can be done with the automatic mesh generation. In ATENA, three main options exist for the FE mesh. Out of these three options, structured mesh is used in this study because it consists of only brick element. The FE mesh is done by accessing the FE mesh item in the input data access tree. FE mesh required the mesh generation parameter or the mesh size. After giving the mesh size, FE mesh is automatically generated. When the FE mesh is done, apply the load and supports. Here, I had applied the incremental load in terms of prescribed deflection of 70 steps to get the load correspondingly the prescribed deformation at each step. At last, choose the monitoring points. The monitored data can provide important information about the state of the structure and also it is allow us to monitor the load deflection graph during the non-linear finite element analysis. After all these steps, FE modelling of the beam is completed except the analysis. The FE model of the control beam and stressed retrofitted beam is shown in figure 3.14 and figure 3.15

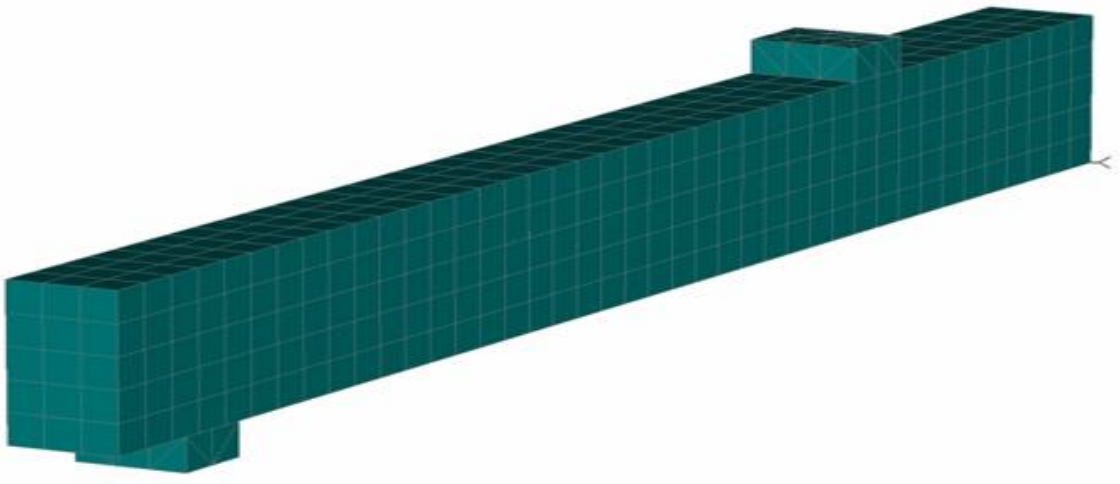

Figure 3.14 FE model of the Control Beam

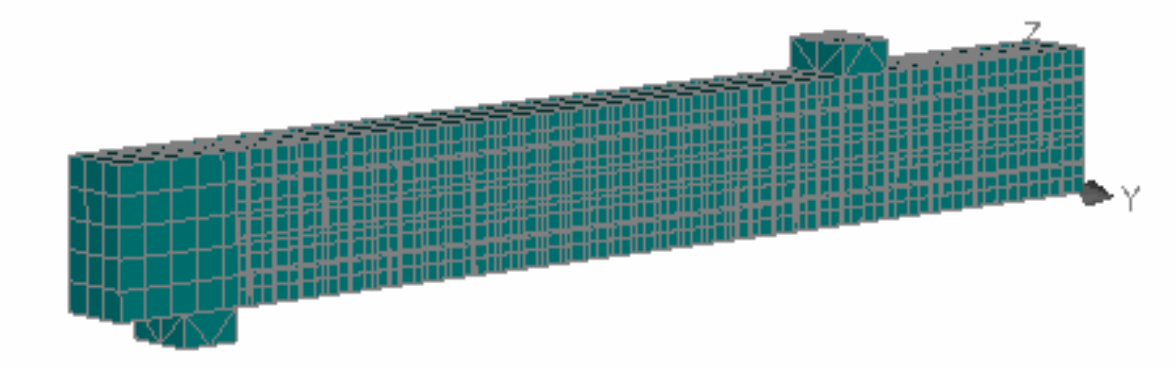

Figure 3.15 FE model of the Stressed Retrofitted Beam

When the FE model had created, it is ready to start the analysis. The FE non-linear analysis is done in Run window. The FE non-linear static analysis calculates the effects of steady loading conditions on a structure, while ignoring inertia and damping effects, such as those caused by time-varying loads. A static analysis can, however, include steady inertia loads (such as gravity and rotational velocity), and time-varying loads that can be approximated as static equivalent loads (such as the static equivalent wind and seismic loads commonly defined in many building codes).

Static analysis is used to determine the displacements, stresses, strains, and forces in structures or components by loads that do not induce significant inertia and damping effects.

When the FE non linear static analysis is completed the, the results shown in third part of the ATENA i.e post-processing. Here, all the results are shown. The stress- strain values at every step, crack pattern, cracks propagation at every step shown which helps in to analyze the behaviour of the beam at every step of load deflection. This all can be done in ATENA.

The best part of the ATENA is the simpler way of solving the non-linear structural behaviour through finite element method and its incremental loading criteria. Different methods are available in ATENA for solving non-linear equations which help in FE modelling, such as, linear method, Newton-Raphson Method, Modified Newton-Raphson Method, Arc Length Method etc are used in ATENA.

Among these the Newton-Raphson Method and Modified Newton-Raphson Method is more commonly used method. In our present study, Newton-Raphson method is used for solving the simultaneous equations. It is an iterative process of solving the non-linear equations.

3.10 Incremental Loading and Equilibrium Iterations

One approach to nonlinear solutions is to break the load into a series of load increments. The load increments can be applied either over several load steps or over several sub steps within a load step. At the completion of each incremental solution, the program adjusts the stiffness matrix to reflect the nonlinear changes in structural stiffness before proceeding to the next load increment. .

The ATENA program overcomes this difficulty by using Full Newton-Raphson method, or Modified Newton-Raphson method, which drive the solution to equilibrium convergence (within some tolerance limit) at the end of each load increment.

In Full Newton-Raphson method, it obtains the following set of non-linear equations:

$$K(p)\,\Delta p = q - f(p)$$

where:

q is the vector of total applied joint loads,

$f(p)$is the vector of internal joint forces,

Δp is the deformation increment due to loading increment,

p are the deformations of structure prior to load increment,

$\boldsymbol{K}(p)$ is the stiffness matrix, relating loading increments to deformation increments.

Figure 4.3 illustrates the use of Newton-Raphson equilibrium iterations in nonlinear analysis. Before each solution, the Newton-Raphson method evaluates the out-of -balance load vector, which is the difference between the restoring forces (the loads corresponding to the element stresses) and the applied loads. The program then performs a linear solution, using the out-of -balance loads, and checks for convergence. If convergence criteria are not satisfied, the out-of-balance load vector is re-evaluated, the stiffness matrix is updated, and a new solution is obtained. This iterative procedure continues until the problem converges.

But sometimes, the most time consuming part of the Full Newton-Raphson method solution is the re-calculation of the stiffness matrix $\boldsymbol{K}(pi-1)$ at each iteration. In many cases this is not necessary and we can use matrix $\boldsymbol{K}(p0)$ from the first iteration of the step. This is the basic

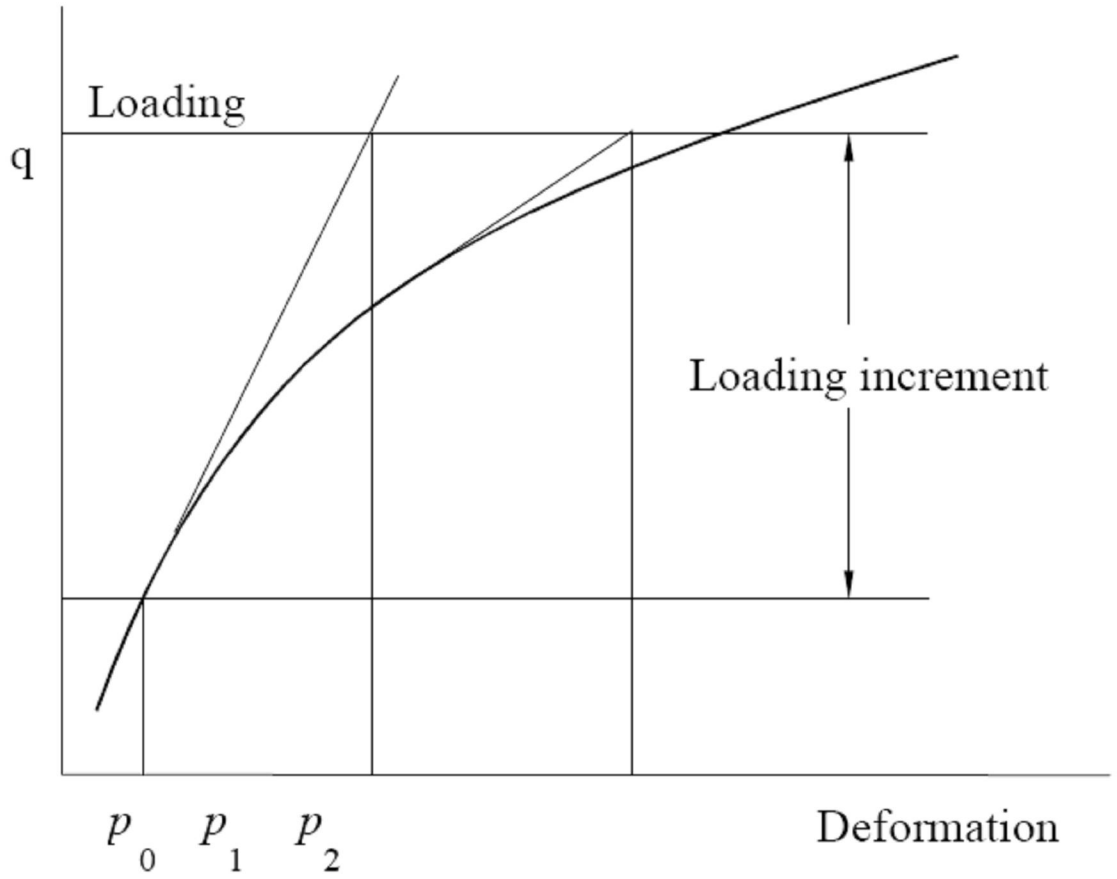

Figure 3.15 Full Newton-Raphson Method

idea of the so-called Modified Newton-Raphson method. It produces very significant time saving, but on the other hand, it also exhibits worse convergence of the solution procedure. The simplification adopted in the Modified Newton-Raphson method can be mathematically expressed by:

$$K\,(p_i{-}1) = K\,(p_0)$$

The modified Newton-Raphson method is shown in Fig. 3.16. Comparing Fig. 3.15 and Fig. 3.16, it is apparent that the Modified Newton-Raphson method converges more slowly than the original Full Newton-Raphson method. On the other hand a single iteration costs less computing time, because it is necessary to assemble and eliminate the stiffness matrix only once. In practice

a careful balance of the two methods is usually adopted in order to produce the best performance for a particular case. Usually, it is recommended to start a solution with the original Newton-Raphson method and later, i.e. near extreme points, switch to the modified procedure to avoid divergence. .

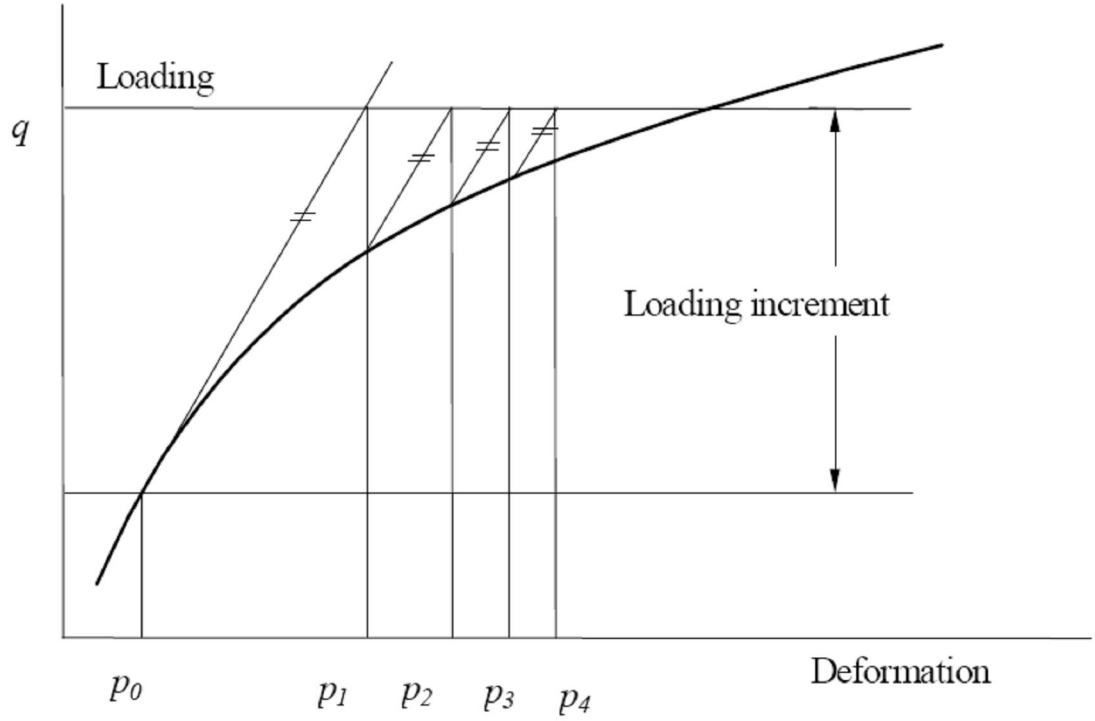

Figure 3.16 Modified Newton-Raphson Method

CHAPTER 4
RESULTS AND DISCUSSION

4.1 General

The present chapter discussed the analytical results of control RCC beams and the stressed retrofitted RCC beams to 60%, 75% & 90% of the ultimate load with GFRP under the static two point loads have been analyzed using ATENA. These results are further compared with experimental results. Load deflection curve and the cracking behaviour can also be discussed in this chapter.

4.2 FEM Analysis of the Control Beam

In the analysis, the modelling of the half control beam due to symmetry of the load and the shape can be done by finite element method using ATENA shown in fig 4.1. In ATENA, load can be applied in terms of prescribed deformation and get the loads corresponding to the deformation. Results can be seen in ATENA by post processing. The load deflection curves and the cracking behaviour in the beam obtained analytically using ATENA. Typical results obtained from FEM formulation in terms of deflection and load for the RCC beam. The beam size and the material properties which are used in the modelling of the control beam are same as of Goyal (2007) thesis report. The characteristic of the control beam is studied at each step. The ultimate load for the controlled half beam was found out to be 19.9KN and the ultimate deflection was found out to be 43.5mm.

For the specimen in general, at the early stages of loading the behaviour was elastic until the appearance of the first crack. Invariably, the crack was initiated at the centre of the beam and the cracks gradually propagate towards the end supports on the tension face side as the loading progressed.

Analytical result for control beam is given in table 4.1 at every steps and load deflection curve is given in fig 4.2.

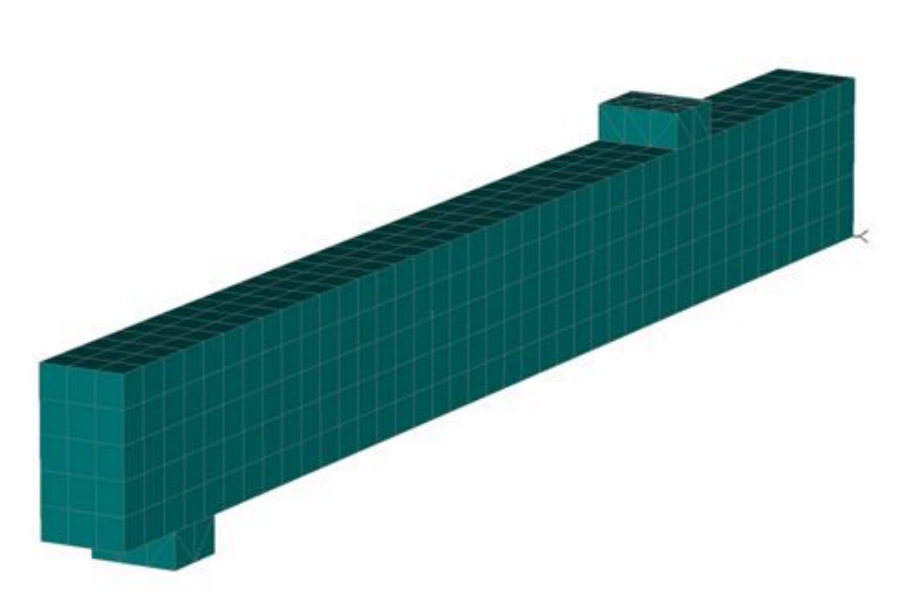

Figure 4.1 Finite Element Model of the Control Beam

Table 4.1 Analytical Results for Control Beam

Step	Load in KN	Deflection in m
1	1.395E-03	7.135E-04
2	2.789E-03	1.427E-03
3	3.542E-03	2.171E-03
4	4.568E-03	6.593E-03
5	5.484E-03	9.423E-03
6	6.603E-03	1.226E-02
7	6.810E-03	1.295E-02
8	7.612E-03	1.508E-02
9	7.877E-03	1.579E-02
10	8.474E-03	1.724E-02
11	8.971E-03	1.866E-02

12	9.282E-03	1.938E-02
13	9.585E-03	2.010E-02
14	9.695E-03	2.171E-02
15	9.740E-03	2.492E-02
16	9.852E-03	3.026E-02
17	9.882E-03	3.411E-02
18	9.909E-03	3.800E-02
19	9.943E-03	3.877E-02
20	9.955E-03	4.343E-02
21	9.946E-03	4.421E-02
22	9.916E-03	5.045E-02

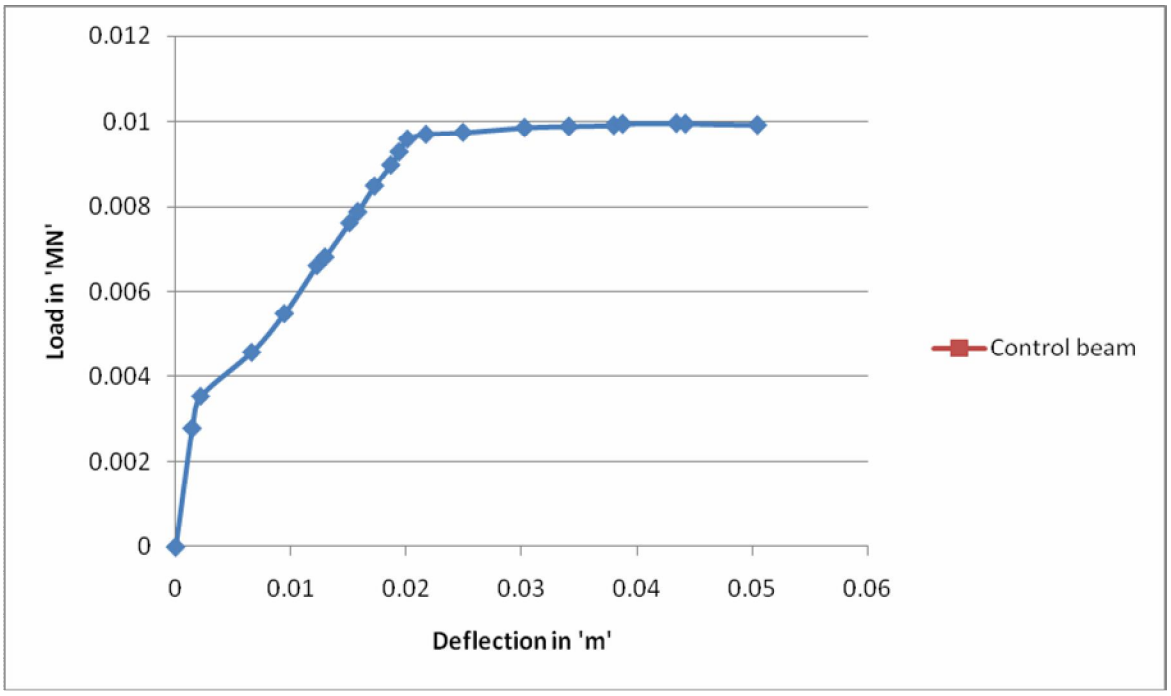

Figure 4.2 Load vs Deflection Curve for Control Beam

The appearance of first crack shows at third step and keeps on increasing as the load and the deflection increases. Fig 4.3 shows the first crack. The maximum crack width is 0.02 mm.

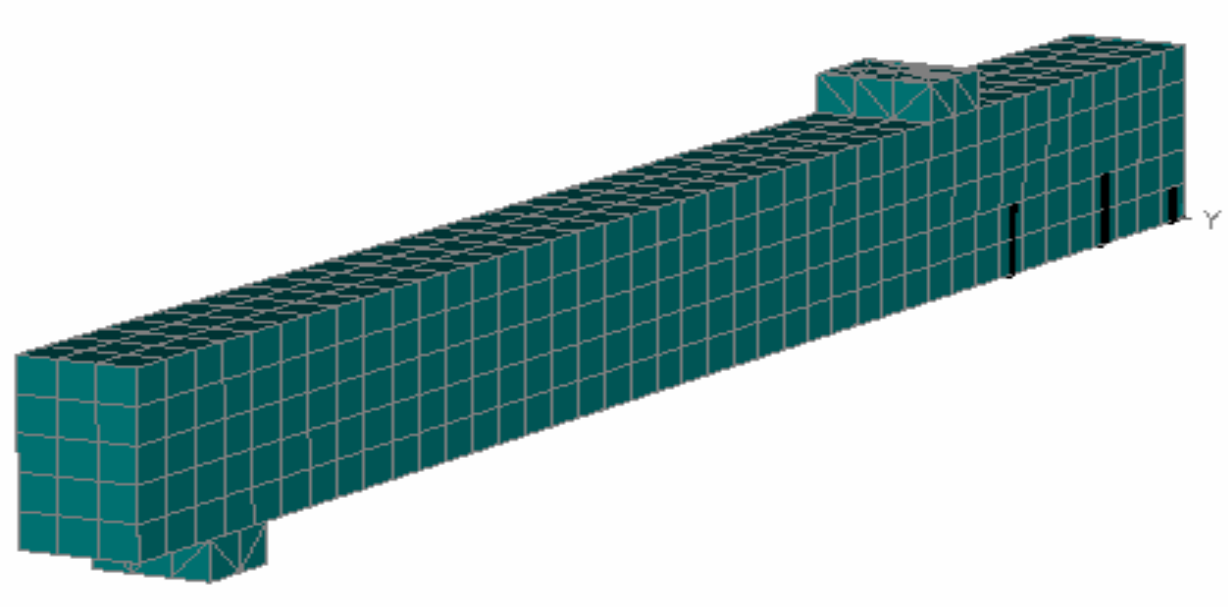

Fig 4.3 Cracks Pattern at 3rd Step of Control Beam

At the 20th step cracks propagate in tension face moves towards the end support and reaches the compression zone shown in fig 4.4. The maximum crack width is 0.165mm.

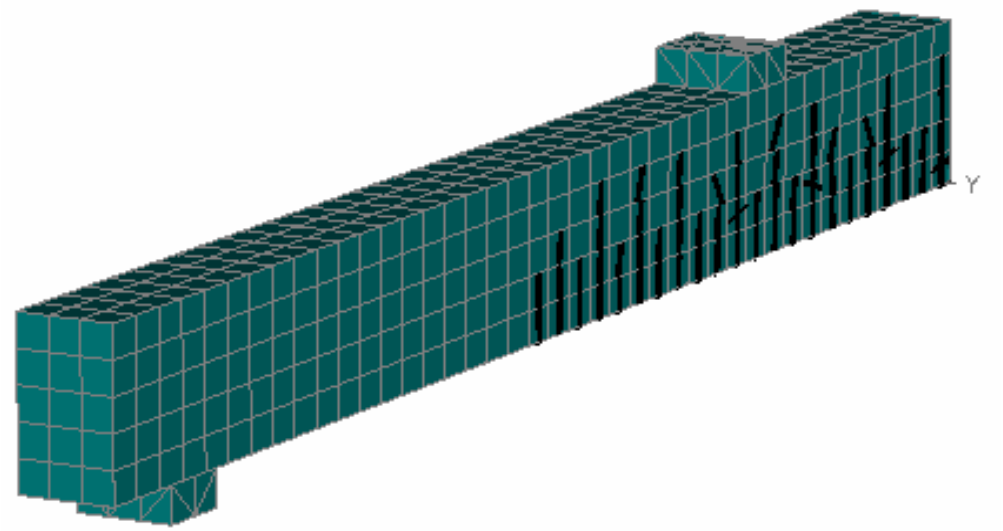

Fig 4.4 Crack Pattern at 20th Step of Control Beam

At the 40th step cracks propagate in tension face moves towards the end support and start cracking and also propagate in the compression zone shown in fig 4.5. The max crack width is 0.525mm.

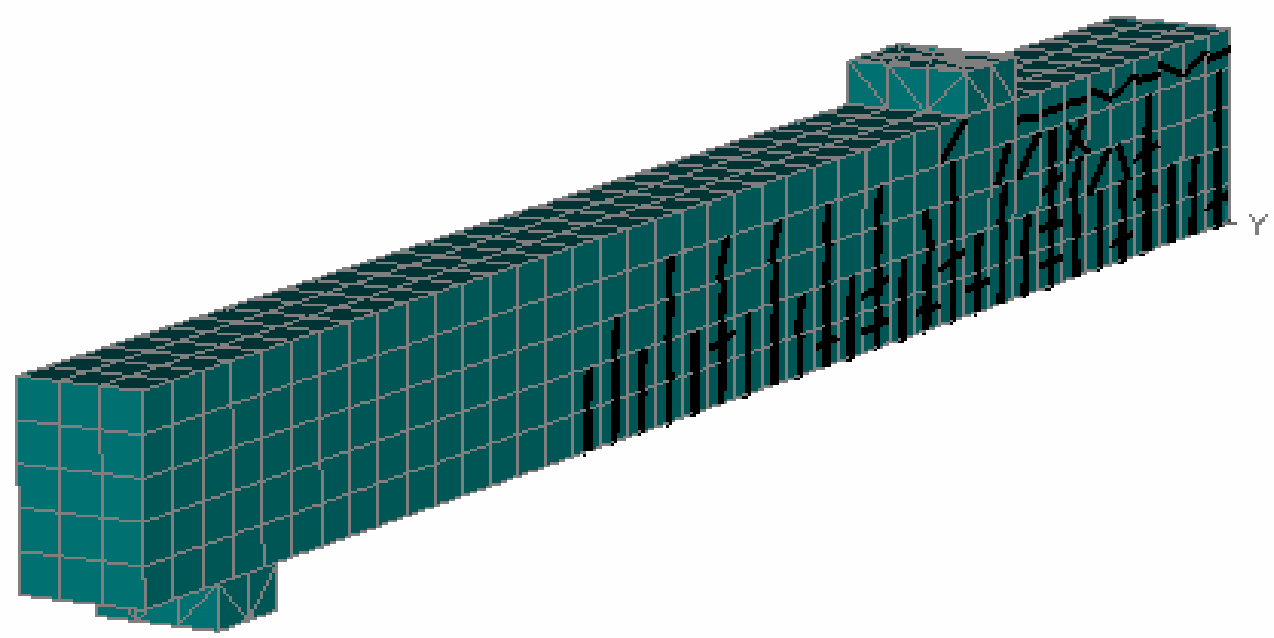

Fig 4.5 Crack Pattern at 40th Step of Control Beam

At the 58th step when we get the ultimate load and the ultimate deflection, cracks keeps on increasing as shown in Fig 4.6. The maximum crack width is 0.918mm.

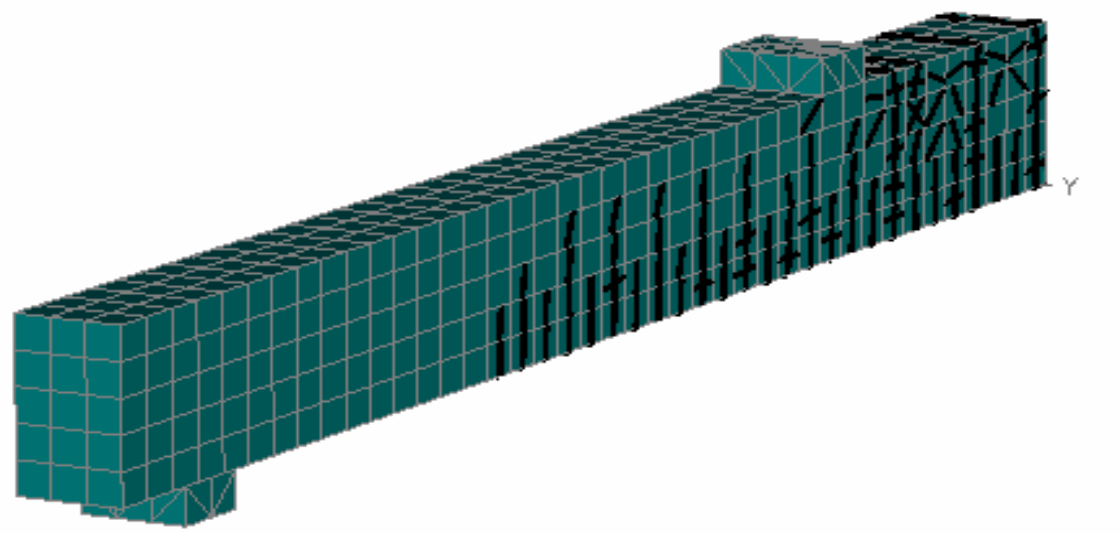

Fig 4.6 Crack Pattern at 58th Step of Control Beam

4.3 Comparison between the Analytical results and the Experimental results of the control beam

Table 4.2 Comparison of the Control Beam Results

S No.	Analytical Results		Experimental Results	
	Load (KN)	Deflection (mm)	Load (KN)	Deflection (mm)
1	0	0	0	0
2	5.6	1.42	4.2	4.5
3	8.4	4.44	8.4	5.8
4	13.2	12.26	12.4	16.4
5	15.2	15.08	13.5	17.1
6	19.9	43.43	16.4	42

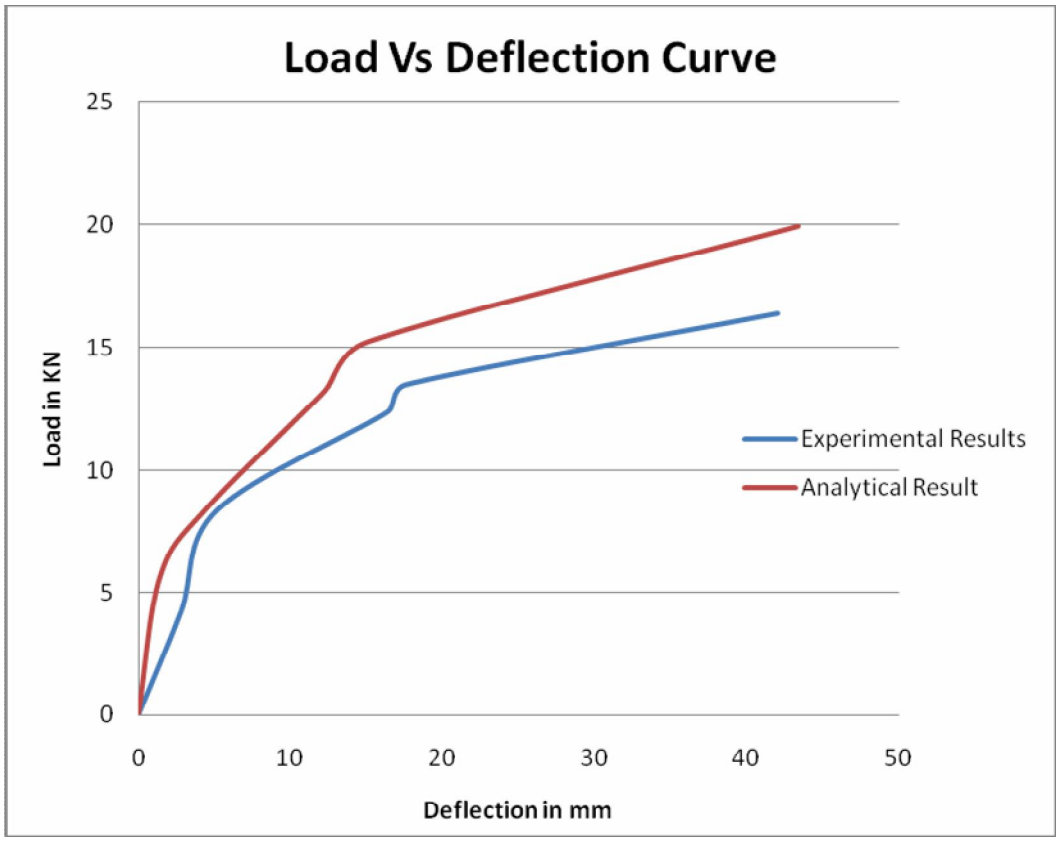

FIGURE 4.7 Compared Load vs Deflection curve for Control Beam

Fig 4.7 and table 4.2 shows the comparison between the experimental results and the analytical results.

From above all the data and graph, the result came from the analytical data vary as compared to the experimental data. The ultimate load and the ultimate deflection came from the analytical result are 19.9KN and 43.43mm respectively whereas the ultimate load and the ultimate deflection came from the experimental result was 16.4KN and 42mm respectively.
When analyze these data, the analytical results shows the load is increased by nearly 4KN whereas deflection increases slightly nearly 1.5mm as compared to the experimental results. That means analysis gives good results as compared to the experimental result.

4.4 FEM Analysis of the Stressed Retrofitted Beams and their comparison with control beam.

As in the experiment, the three beams were stressed at different % i.e. 60%, 75%, and 90%of the ultimate load carried by the control beams results and then these beams are strengthened by using GFRP sheets. In this study, same work can be done analytically and compared the analytical results with the experimental results. Firstly, the three stressed half beams were modelled due to the shape and the loading at the same % as shown in fig 4.8 but according to ultimate load of the control beam came from the analytical result and done the analysis to get the results. The results came out from all these three beams. The analytical results obtained from 60% stressed retrofitted half beam, the ultimate load and the ultimate deflection was 16.9KN and 119.6mm respectively. Similarly analytical results were obtained for the other two stressed retrofitted beams at 75% and 90%. Table 4.3, 4.4 and 4.5 and fig 4.9, 4.10 and 4.11 shows the analytical values and curves of the stressed retrofitted beams at 60%, 75% and 90% respectively.

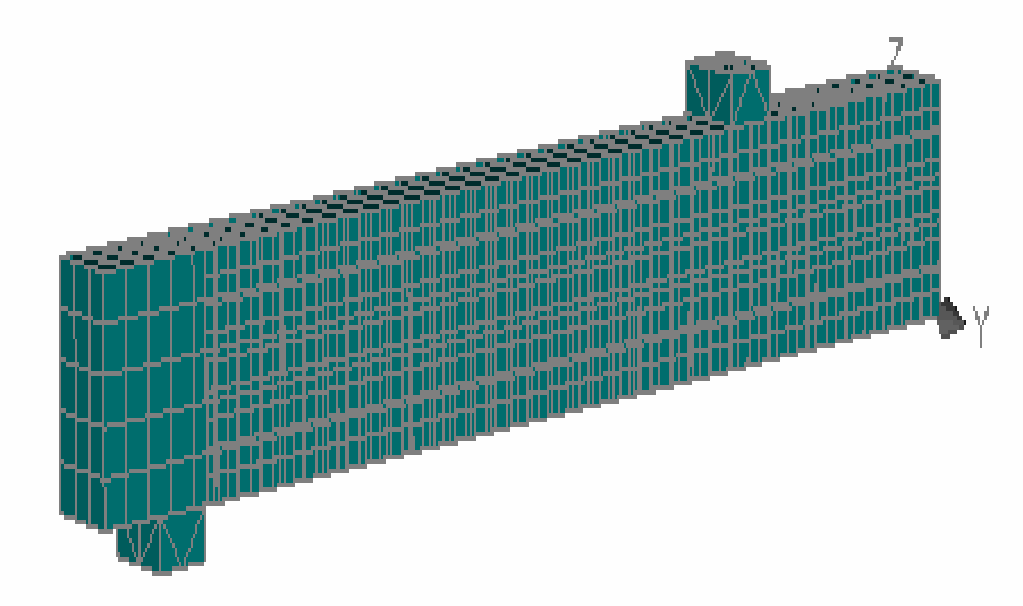

Figure 4.8 FE Model of the Stressed Retrofitted Beam

Table 4.3 Analytical Results for 60% Stressed Retrofitted Beams

Step	Load in MN	Deflection in m
1	1.471E-03	4.204E-03
2	2.941E-03	8.407E-03
3	3.674E-03	1.051E-02
4	4.407E-03	1.261E-02
5	5.872E-03	1.681E-02
6	6.603E-03	1.891E-02
7	7.334E-03	2.101E-02
8	8.794E-03	2.521E-02
9	9.523E-03	2.731E-02
10	1.061E-02	3.161E-02

11	1.131E-02	3.372E-02
12	1.191E-02	3.814E-02
13	1.288E-02	4.900E-02
14	1.375E-02	5.991E-02
15	1.446E-02	6.858E-02
16	1.494E-02	7.504E-02
17	1.523E-02	7.927E-02
18	1.556E-02	8.356E-02
19	1.596E-02	9.019E-02
20	1.632E-02	9.888E-02
21	1.669E-02	1.078E-01
22	1.672E-02	1.102E-01
23	1.679E-02	1.149E-01
24	1.686E-02	1.196E-01
25	1.685E-02	1.221E-01
26	1.675E-02	1.247E-01

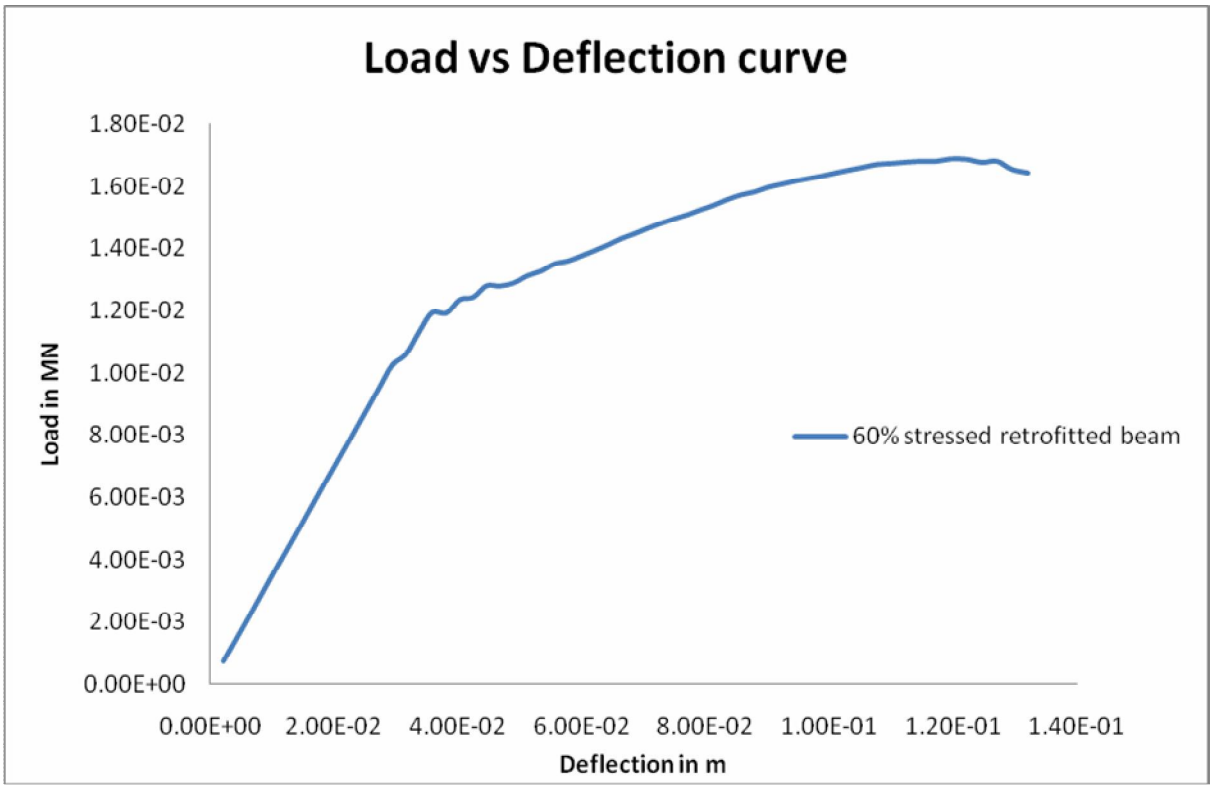

Figure 4.9 Load vs Deflection curve for 60% Stressed Retrofitted Beam

Table 4.4 Analytical Results for 75% Stressed Retrofitted Beam

Step	Load in MN	Deflection in m
1	-1.542E-03	-4.733E-03
2	-2.696E-03	-8.282E-03
3	-3.849E-03	-1.183E-02
4	-4.617E-03	-1.420E-02
5	-5.768E-03	-1.775E-02
6	-6.534E-03	-2.011E-02
7	-7.682E-03	-2.366E-02

8	-8.447E-03	-2.602E-02
9	-9.592E-03	-2.957E-02
10	-1.074E-02	-3.312E-02
11	-1.150E-02	-3.548E-02
12	-1.262E-02	-4.425E-02
13	-1.368E-02	-5.805E-02
14	-1.447E-02	-7.121E-02
15	-1.563E-02	-8.951E-02
16	-1.584E-02	-9.320E-02
17	-1.597E-02	-9.679E-02
18	-1.619E-02	-1.018E-01
19	-1.634E-02	-1.056E-01
20	-1.639E-02	-1.069E-01
21	-1.643E-02	-1.082E-01
22	-1.655E-02	-1.111E-01
23	-1.656E-02	-1.124E-01
24	-1.663E-02	-1.139E-01
25	-1.676E-02	-1.151E-01
26	-1.663E-02	-1.162E-01
27	-1.658E-02	-1.168E-01
28	-1.659E-02	-1.176E-01

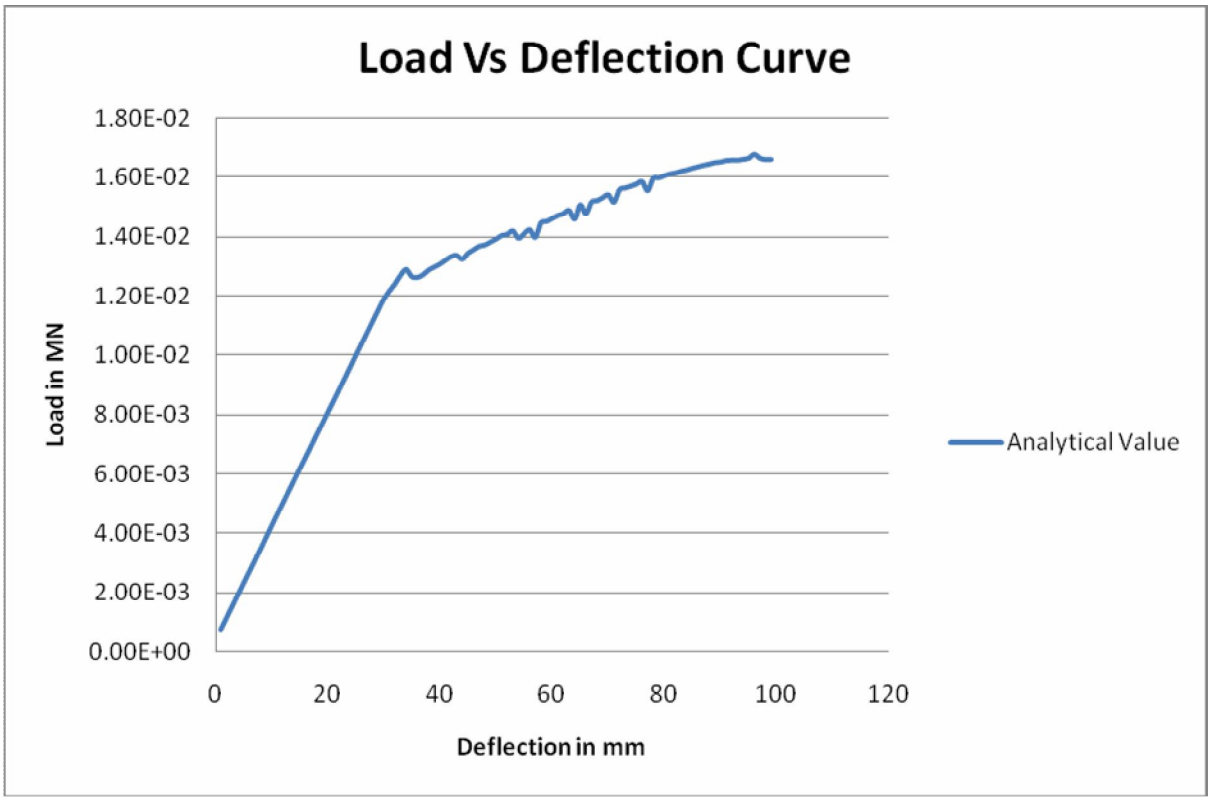

Figure 4.10 Load vs Deflection curve for 75% Stressed Retrofitted Beam

Table 4.5 Analytical Result for 90% Stressed Retrofitted Beam

Steps	Load in MN	Deflection in m
1	1.877E-03	-6.566E-03
2	2.814E-03	-9.848E-03
3	3.750E-03	-1.313E-02
4	4.685E-03	-1.641E-02
5	5.618E-03	-1.969E-02
6	6.551E-03	-2.297E-02
7	7.948E-03	-2.790E-02

8	8.878E-03	-3.118E-02
9	9.807E-03	-3.446E-02
10	1.073E-02	-3.774E-02
11	1.155E-02	-4.104E-02
12	1.270E-02	-4.781E-02
13	1.369E-02	-5.643E-02
14	1.410E-02	-7.064E-02
15	1.449E-02	-7.908E-02
16	1.461E-02	-8.078E-02
17	1.474E-02	-8.247E-02
18	1.484E-02	-8.415E-02
19	1.496E-02	-8.583E-02
20	1.503E-02	-8.750E-02
21	1.510E-02	-8.922E-02
22	1.523E-02	-9.092E-02
23	1.535E-02	-9.158E-02
24	1.542E-02	-9.224E-02
25	1.551E-02	-9.393E-02
26	1.563E-02	-9.564E-02
27	1.576E-02	-9.632E-02
28	1.558E-02	-9.910E-02

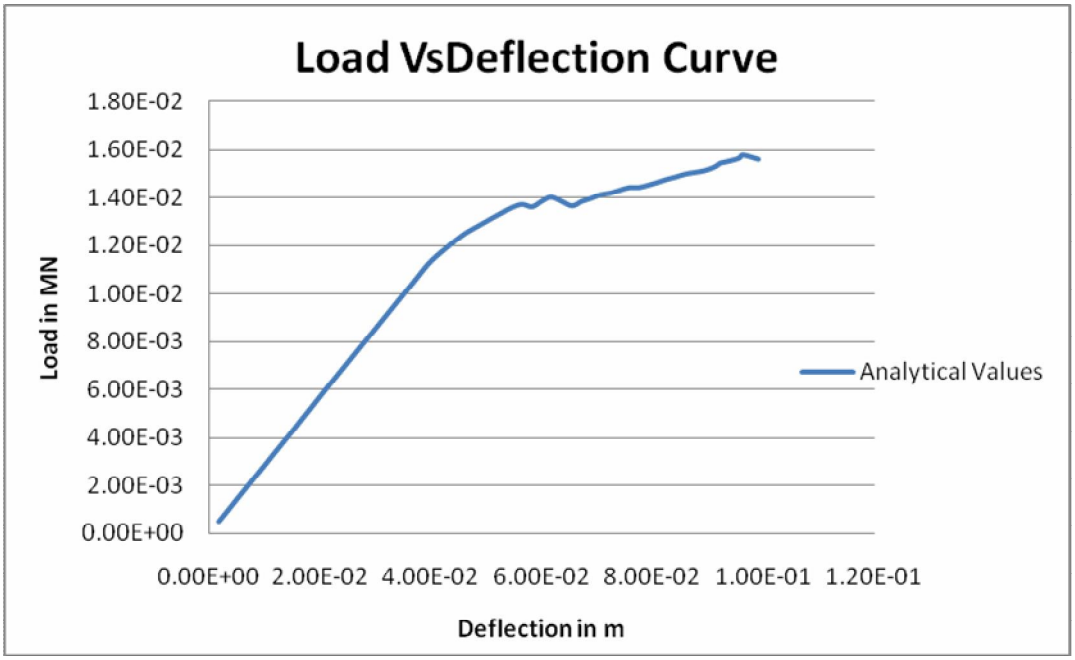

Figure 4.11 Load vs Deflection curve for 90% Stressed Retrofitted Beam

From above all the data, ultimate load and the ultimate deflection of the stressed retrofitted beams were much higher than the control beam.

For the 60% stressed retrofitted beam were 34KN and 119.6mm respectively was increased load by 70% as compared to the control beam and also higher the crack width.

For the 75% stressed retrofitted beam were 33.6KN and 115.1mm respectively was increased load by 67.35% as compared to the control beam and also higher the crack width.

For the 90% stressed retrofitted beam were 31.6KN and 96.3mm respectively was increased load by 57.7% as compared to the control beam but nearly same crack width.

Now let us see the cracking behaviour of the stressed retrofitted beams at 60%, 75% and 90%. Here we can see the propagation of the cracks, its crack pattern and crack width at different steps.

At 60% stressed retrofitted beam, crack initiated at 15^{th} step when the ultimate load was 10.61KN and the ultimate deflection was 31.61mm was shown in fig 4.12. The crack width was 0.132mm.

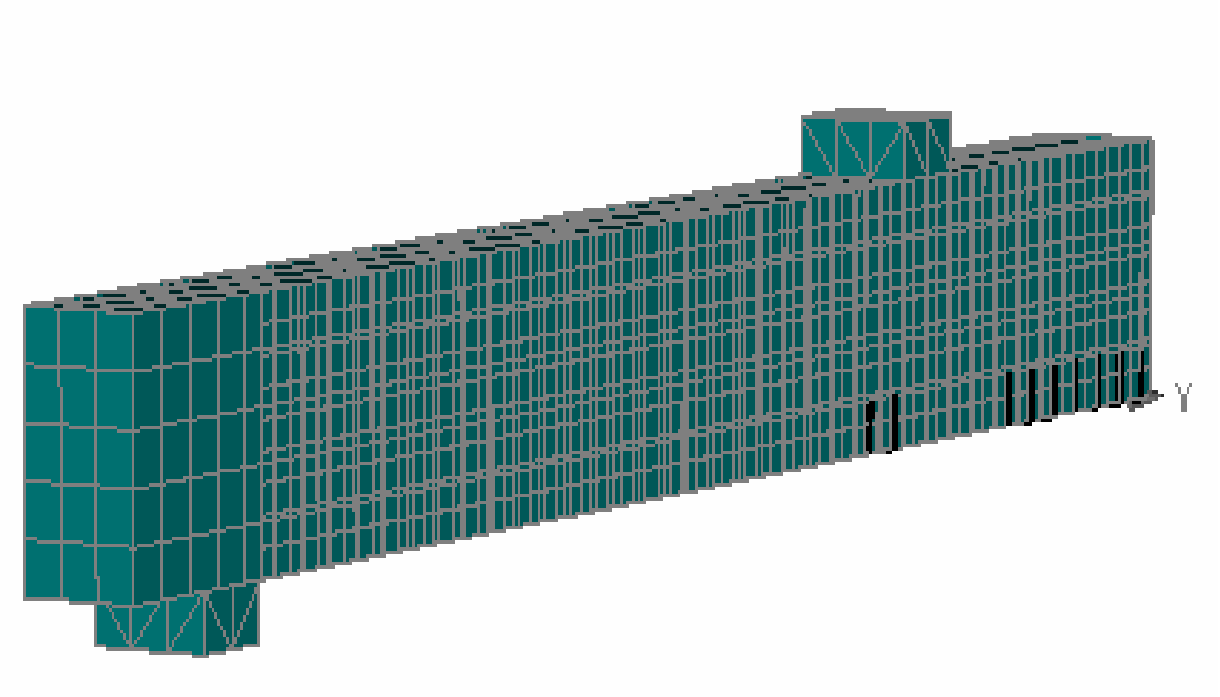

Figure 4.12 Crack Pattern at 15th step of 60% Stressed Retrofitted Beam

At 75% stressed retrofitted beam, crack initiated at 32nd step when the ultimate load was 12.16KN and the ultimate deflection was 37.92mm was shown in fig 4.13. The crack width was 0.184mm.

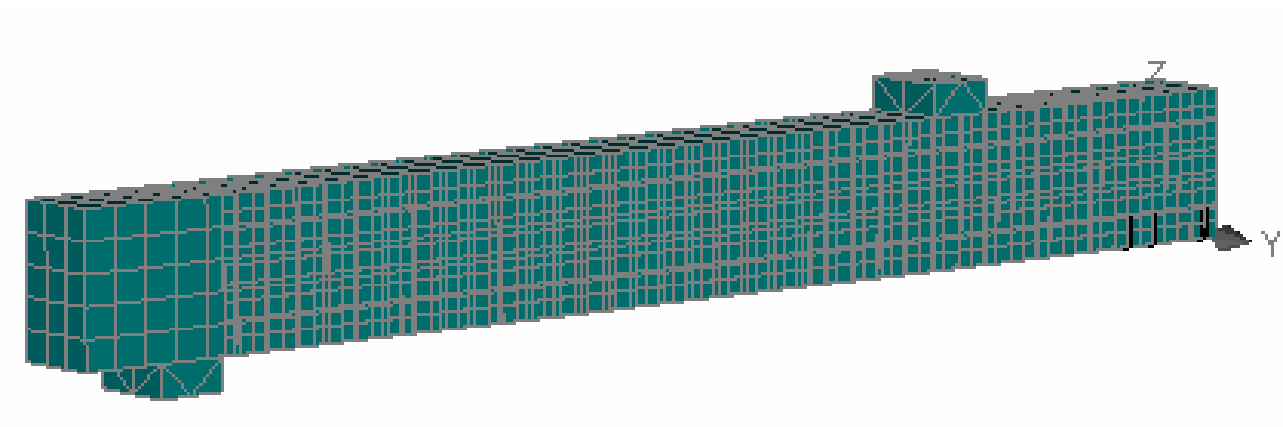

Figure 4.13 Crack Pattern at 32nd step of 75% Stressed Retrofitted Beam

At 90% stressed retrofitted beam, crack initiated at 34nd step when the ultimate load was 13.69KN and the ultimate deflection was 56.69mm was shown in fig 4.14. The crack width was 0.293mm.

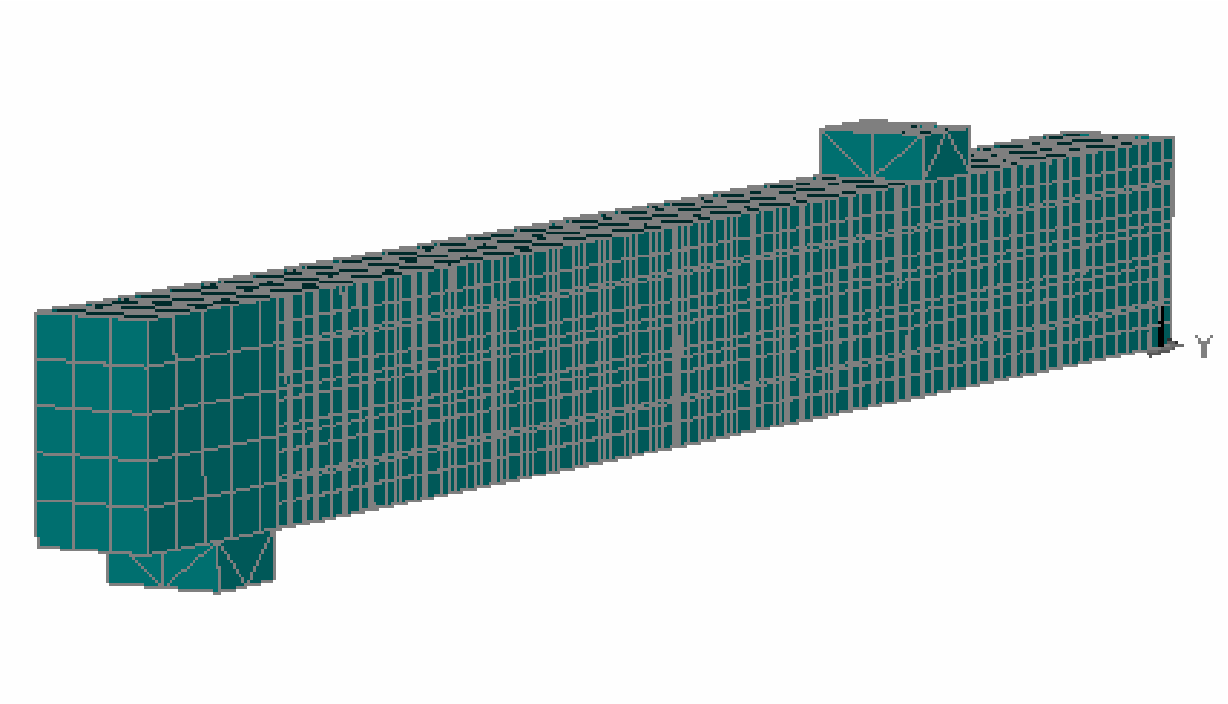

Figure 4.14 Crack Pattern at 34th step of 90% Stressed Retrofitted Beam

Now, we can check the cracking behaviour of the stressed retrofitted beam when the load and the corresponding deflection at maximum.

At 60% stressed retrofitted beam, the ultimate load was 16.9KN and corresponding ultimate deflection was 119.6mm. The crack width was 2mm. The cracks increases in upward direction and moves towards the end support of the beam. The maximum cracks found at the centre of the beam. Fig 4.15 shows the detailed cracking behaviour of the 60% stressed retrofitted beam.

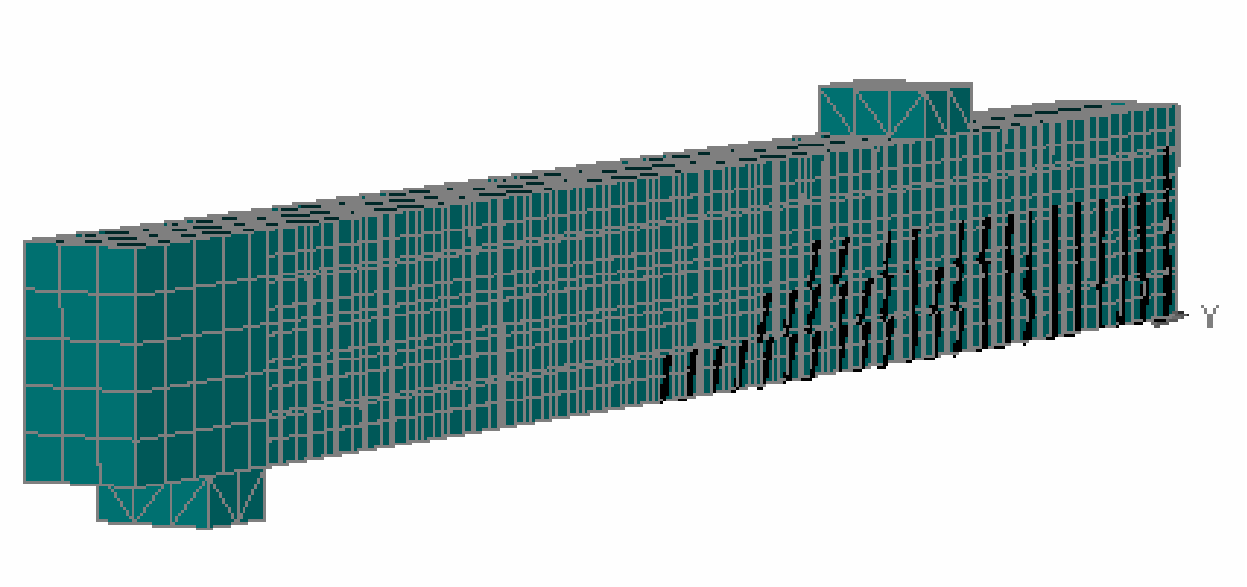

Figure 4.15 Crack Pattern at 55th step of 60% Stressed Retrofitted Beam

At 75% stressed retrofitted beam, the ultimate load was 16.66KN and corresponding ultimate deflection was 118.4mm. The crack width was 1.7mm. The cracks increases slightly in upward direction and moves towards the end support of the beam. The maximum cracks found at the centre of the beam. Fig 4.16 shows the detailed cracking behaviour of the 75% stressed retrofitted beam.

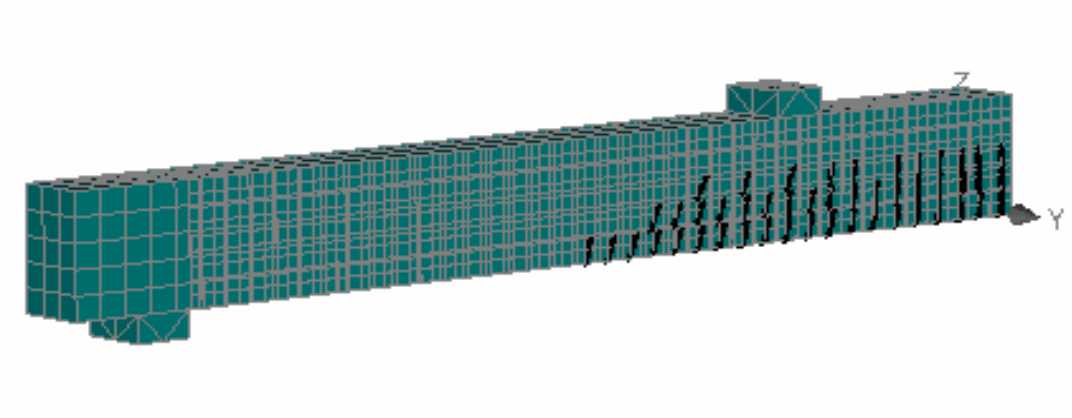

Figure 4.16 Crack Pattern at 97th step of 75% Stressed Retrofitted Beam

At 90% stressed retrofitted beam, the ultimate load was 15.7KN and corresponding ultimate deflection was 99.3mm. The crack width was 0.943mm. The cracks increases in upward direction and moves towards the end support of the beam. As compared to the other beams, it appeared less cracks and crack width. The maximum cracks found at the centre of the beam. Fig 4.17 shows the detailed cracking behaviour of the 90% stressed retrofitted beam.

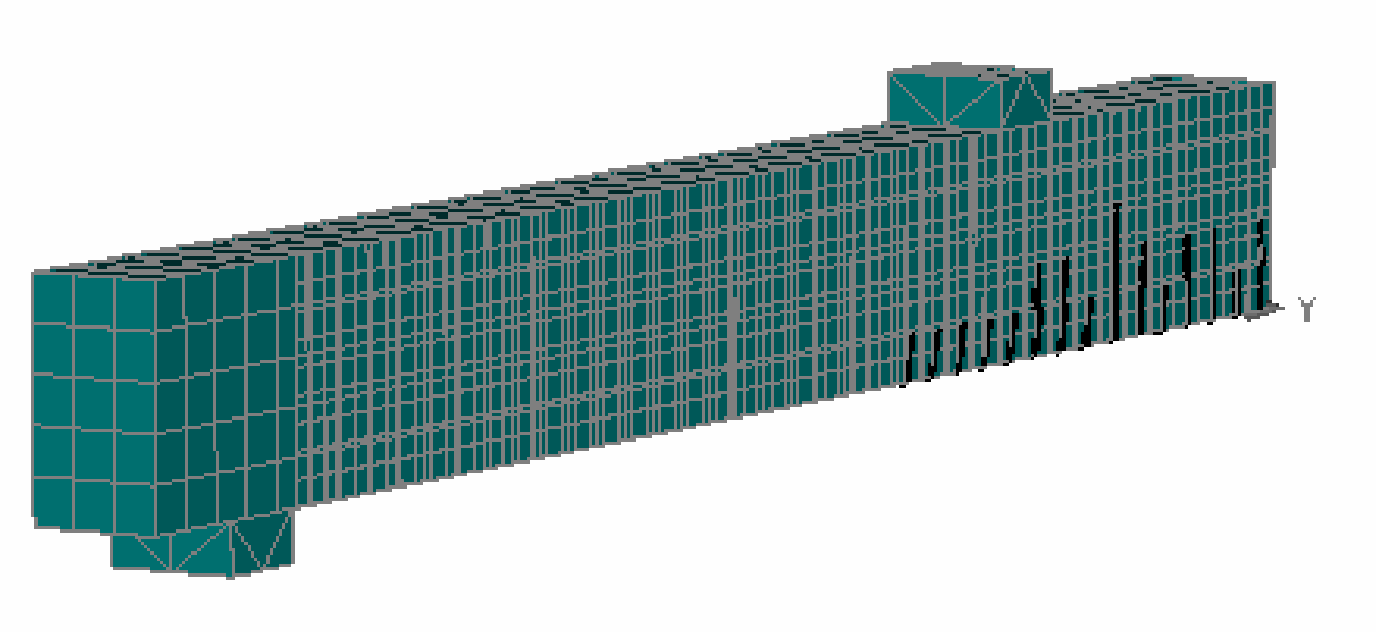

Figure 4.17 Crack Pattern at 59th step of 90% Stressed Retrofitted Beam

4.5 Comparison between the Analytical results and the Experimental results of the Stressed Retrofitted Beams.

1. ***60% Stressed Retrofitted Beam***

Table 4.6 Comparison of the 60% Stressed Retrofitted Beam Results

S No.	Analytical Results		Experimental Results	
	Load (KN)	Deflection (mm)	Load (KN)	Deflection (mm)
1	0	0	0	0
2	4.4	6.3	4.2	3
3	8.8	12.61	8.4	7
4	13.2	18.91	12.4	10.6

5	14.6	21.01	15.1	15
6	17.6	25.21	16.4	18
7	21.2	31.61	26.1	37.5
8	26.5	53.43	30.2	55
9	30.1	77.14	32	67.5
10	34	119.6	34	115

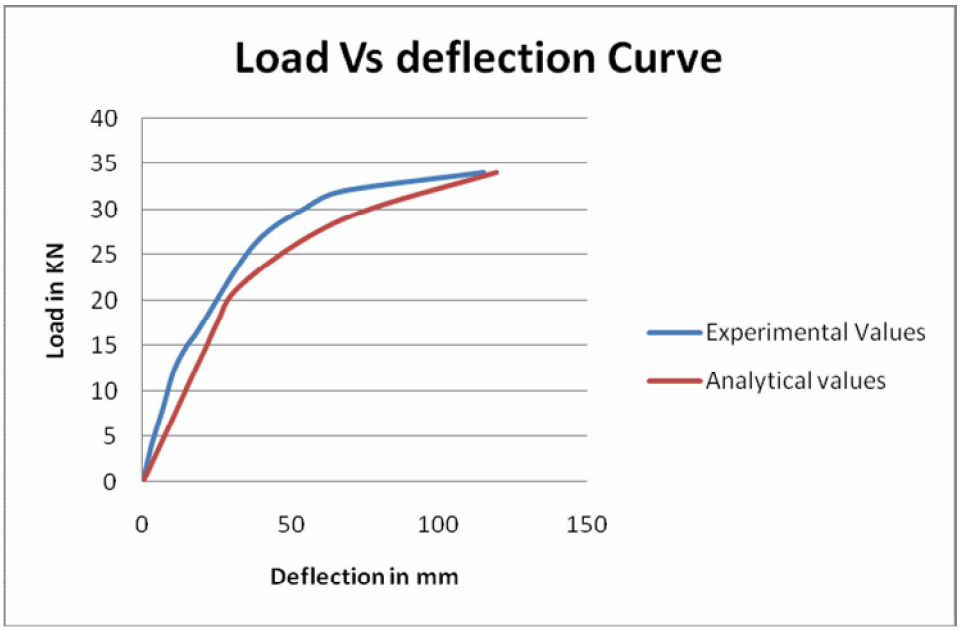

Figure 4.18 Compared Load vs Deflection curve of 60% Stressed Retrofitted Beam

Figure 4.18 and table 4.6 shows the comparison between the experimental results and the analytical results.

From above all the data and graph, the results came from the analytical data and experimental data are very near to each other. The ultimate load and the ultimate deflection came from the analytical result is 34KN and 119.6mm respectively whereas the ultimate load and the ultimate deflection came from the experimental result was 34KN and 115mm respectively. The results obtained from the analysis as well as the experiment shows same ultimate load but slightly variation of 4.5 mm in the ultimate deflection.

2. *75% Stressed Retrofitted Beam*

Table 4.7 Comparison of the 75% Stressed Retrofitted Beam Results

S No.	Analytical Results		Experimental Results	
	Load (KN)	Deflection (mm)	Load (KN)	Deflection (mm)
1	0	0	0	0
2	4.6	7	4.2	4.9
3	8.4	13	8.4	10.1
4	13	20.1	12.4	15
5	15.4	23.66	15.1	18.4
6	16.8	26.02	16.4	21.25
7	24.8	39.13	21.5	43.9
8	30.1	79.85	26.4	55.7
9	32	97.6	30.2	71
10	33.6	115.1	33.7	109.4

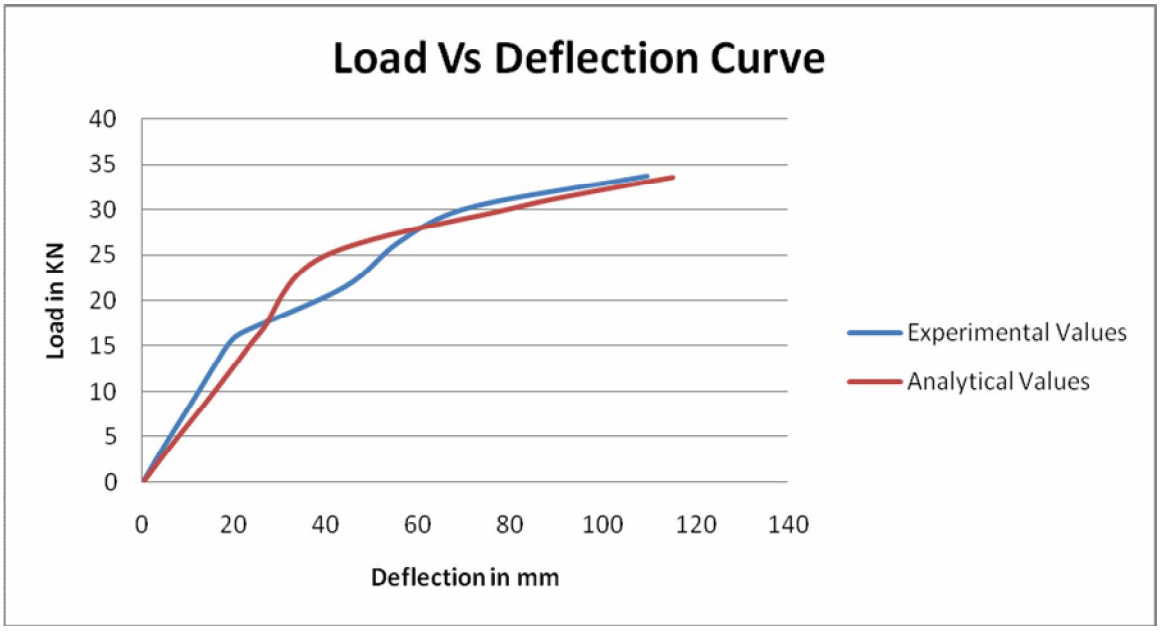

Figure 4.19 Load vs Deflection curve of 75% Stressed Retrofitted Beam

Figure 4.19 and table 4.7shows the comparison between the experimental results and the analytical results.

From above all the data and graph, the result came from the analytical data nearly the same as the experimental data. The ultimate load and the ultimate deflection came from the analytical result is 33.6KN and 115.1mm respectively whereas the ultimate load and the ultimate deflection came from the experimental result was 33.7KN and 109.4mm respectively.

3. ***90% Stressed Retrofitted Beam***

Table 4.8 Comparison of the 90% Stressed Retrofitted Beam Results

S No.	Analytical Results		Experimental Results	
	Load (KN)	Deflection (mm)	Load (KN)	Deflection (mm)
1	0	0	0	0
2	4.6	8.2	4.2	5.2
3	8.4	14.77	8.4	10.9
4	13	23	12.4	16.5
5	16	28	15.1	20.5
6	16.8	29.5	16.4	23
7	23.4	44.2	21.5	36
8	25.6	62.4	26.4	58
9	29	79.8	30.2	79
10	31.6	96.3	32	90

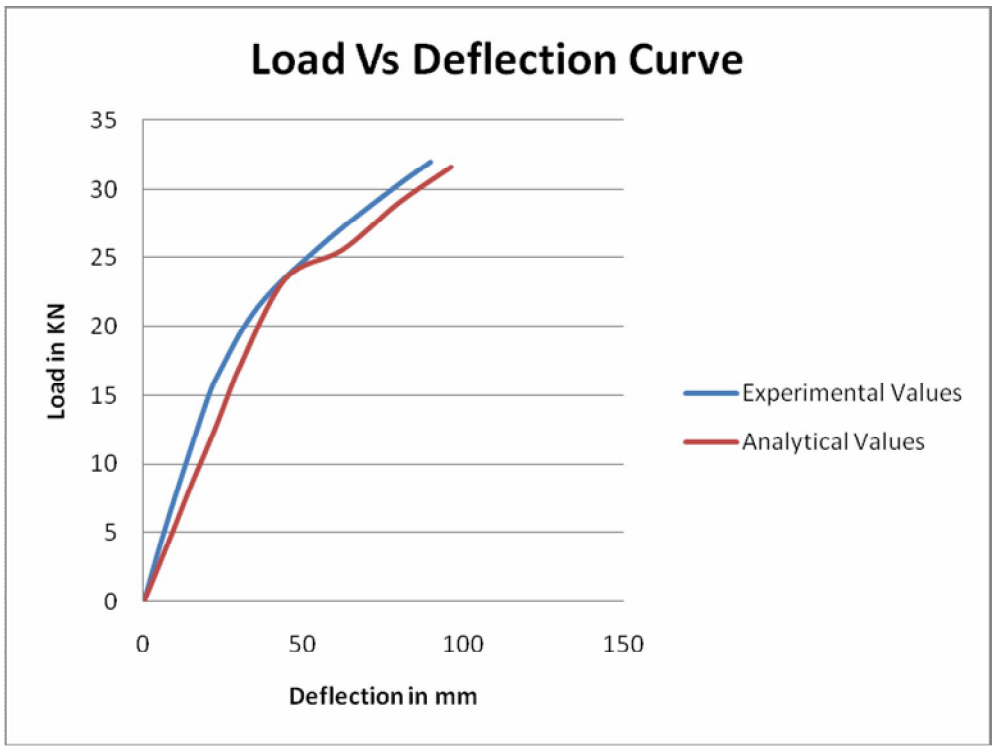

Figure 4.20 Load vs Deflection curve of 90% Stressed Retrofitted Beam

Figure 4.20 and table 4.8 shows the comparison between the experimental results and the analytical results.

From above all the data and graph, the result came from the analytical data nearly the same as the experimental data. The ultimate load and the ultimate deflection came from the analytical result is 31.6KN and 96.3mm respectively whereas the ultimate load and the ultimate deflection came from the experimental result was 32KN and 90mm respectively.

4.6 Comparison between the Control beam and the stressed retrofitted beam at different percentage.

Load deflection curve for control beam and the stressed retrofitted beam has been shown below in fig 4.15.

I. Control beam fails at a load of 9.955 KN with an ultimate deflection of 43.43mm whereas retrofitted stressed beam at 60% fails at a load of 17KN with an ultimate deflection of 119.4mm at the centre showing that there is considerable increase in load

carrying capacity. But control beam has lesser crack width as compared to 60% stressed retrofitted beam. The control beam crack width at the point of ultimate load is 0.9m whereas the crack width of 60% stressed retrofitted beam at the point of ultimate load is 2.07mm.

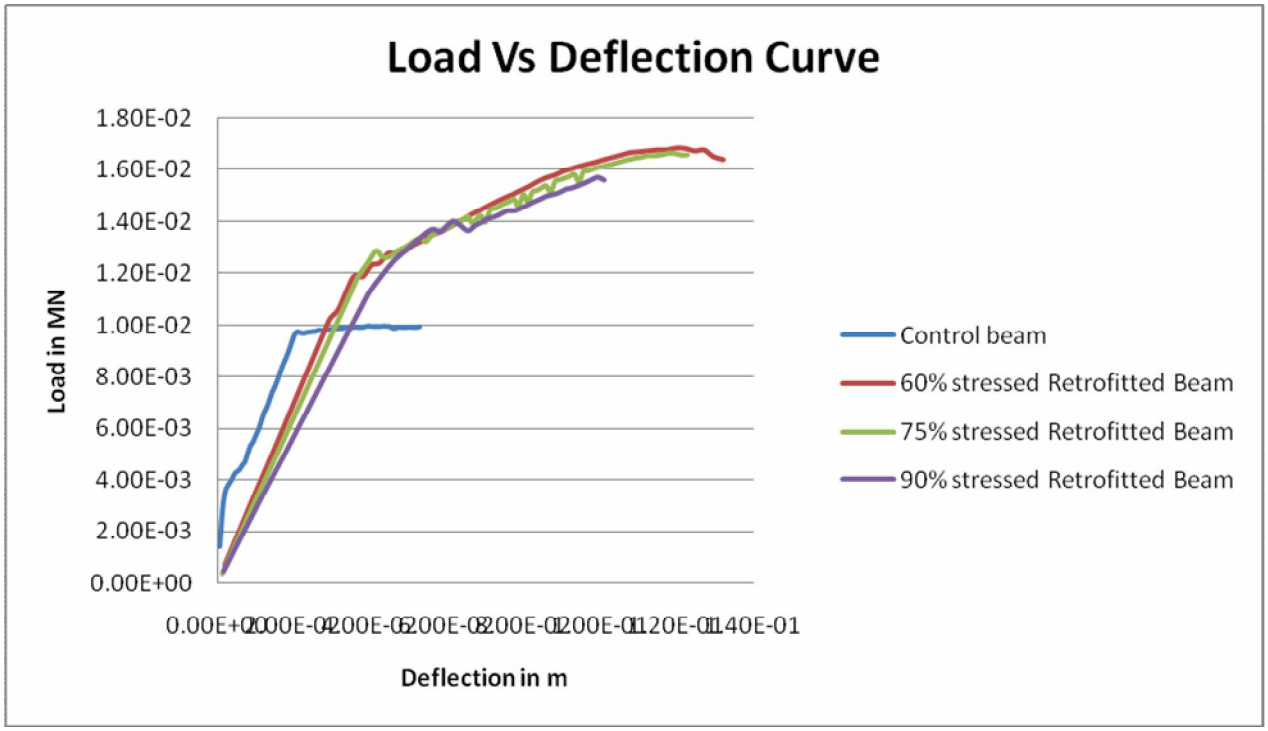

Figure 4.15 Load Vs Deflection Curve for Control Beam and the Stressed Retrofitted Beam at 60%, 75% and 90%.

II. Control beam fails at a load of 9.955 KN with an ultimate deflection of 43.43mm whereas retrofitted stressed beam at 75% fails at a load of 16.8KN with an ultimate deflection of 115.1mm at the centre showing that there is considerable increase in load carrying capacity. But control beam has lesser crack width as compared to 75% stressed retrofitted beam. The control beam crack width at the point of ultimate load is 0.918mm whereas the crack width of 75% stressed retrofitted beam at the point of ultimate load is 1.7mm.

III. Control beam fails at a load of 9.955 KN with an ultimate deflection of 43.43mm whereas retrofitted stressed beam at 90% fails at a load of 15.8KN with an ultimate deflection of 96.4mm at the centre showing that there is considerable increase in load

carrying capacity. But control beam has nearly same crack width as 90% stressed retrofitted beam. The control beam crack width at the point of ultimate load is 0.918mm whereas the crack width of 90% stressed retrofitted beam at the point of ultimate load is 0.943mm.

IV. In comparison to control beam, the beam stressed at 90% of the ultimate load shows linearly variation up to a higher level. This implies that at higher load levels, the load is entirely taken by GFRP.

V. For 60% stressed retrofitted beam, the variation is similar to that of the control beam.

VI. For 75% stressed retrofitted beam, the variation is in between the control beam and the 90% stressed retrofitted beam.

CHAPTER 5
CONCLUSIONS & RECOMMENDATIONS

5.1 GENERAL

An analytical study is carried out for FE modeling of the retrofitted RC beam.

In the first phase of the study, the control beam and the stressed retrofitted beam at 60%, 75% and 90% of the ultimate load of the control beam are modelled in ATENA and their load deflection and cracking behavior is analyzed. Also compare the control beam results with the stressed beam results.

In the second phase of the study is to compare the analytical results with the experimental results.

5.2 CONCLUSIONS

The main conclusions drawn are summarized below:

1. The general behaviour of the finite element models represented by the load-deflection curves show good agreement with the experimental data from the full-scale beam tests.
2. Finite element analysis using non-linear models of cracked concrete, steel bars and FRP is used to predict the behaviour of FRP retrofitted beam. It is verified that the finite element analysis can accurately predict the load deformation, load capacity and cracking behaviour process similar to the experiment.
3. The Analytical result of the control beam was higher by 21% of the Experimental results.
4. The Analytical results of the stressed retrofitted beam at 60%, 75% & 90% of the ultimate load of the control beam show good agreement as the Experimental results.
5. In the analytical results, the Stressed Retrofitted beam at 60%, 75% and 90% of the ultimate load of the control beam was increased by 70%, 67.35% and 57.7% respectively as compared to the control beam.

6. The crack width of the stressed retrofitted beam at 60% and 75% was increased as compared to the control beam and the crack width of the 90% stressed retrofitted beam nearly same as the crack width of the control beam.

5.3 Recommendations

The literature review and analysis procedure utilized in this thesis has provided useful insight for future application of a finite element method for analysis. To ensure that the finite element model is producing good results that can be used for study. FEM model helps in comparing the results with good experimental results data. This will then provide the proper modeling parameters needed for later use. Modelling the RCC beams in FEM based ATENA software gives good results which can be included in future research.

REFERENCES

1. Dat Duthinh and Monica Starnes (2001). Strengthening of Reinforced Concrete Beams with Carbon FRP. Journal of Composites in Constructions, pg 493-498.

2. Damian Kachlakev, PhD, Thomas Miller, PhD, PE; Solomon Yim, PhD and PE; Kasidit Chansawat; Tanarat Potisuk (2001). **FINITE ELEMENT MODELINGOF REINFORCED CONCRETE STRUCTURESSTRENGTHENED WITH FRP LAMINATES, FINAL REPORT.** OREGON DEPARTMENT OF TRANSPORTATION.

3. Z.J. Yang, J.F. Chen and D. Proverbs (2003). **FINITE ELEMENT MODELING OF CONCRETE COVER SEPARATION FAILURE IN FRP PLATED RC BEAMS**. Construction and Building Materials, Vol 17, pg 3-13.

4. R. Perera, A. Recuero, A. De Diego, C. Lopez (2004). **Adherence analysis of fiber reinforced polymer strengthened RC beams.** Journal of Computers and Structures, Vol 82, pg 1865-1873.

5. Supaviriyakit T., Pornpongsaroj P., and Pimanmas A (2004). **FINITE ELEMENT ANALYSIS OF FRP STRENGTHENED RC BEAMS.** Songklanakarin J. Science Technology, Vol 26(4), pg 497-507.

6. R. Santhakumar E. Chandrasekaran and R. Dhanaraj (2004). **ANALYSIS OF RETROFITTED REINFORCED CONCRETE SHEAR BEAMS USING CARBON FIBER COMPOSITES.** Electronic journal of structural engineering, Vol 4, pg 66-74.

7. B Bonfiglioli, A Strauss, G Pascale and K Bergmeister (2005). **Basic study of monitoring onn fibre reinforced polymers: theoretical and experimental study.** Journal of Smart Materials and Structures, Vol 14, pg S12-S23.

8. Giuseppe Simonelli (2005). Report on **Finite Element Analysis of RC Beams retrofitted with Fibre Reinforced Polymers.** Pg 1-220

9. B. Ferracuti, M. Savoia, C. Mazzotti (2006). **A numerical model for FRP-concrete delamination.** Journal of Composites, Vol Part B 37, pg 356-364.

10. Oral Büyüköztürk and Tzu-Yang Yu (2006). **UNDERSTANDING AND ASSESSMENT OF DEBONDING FAILURE IN FRP CONCRETE SYSTEMS.** Seventh International Congress on Advances in Civil Engineering.

11. D. Mostofinejad and S. B. Talaeitaba (2006). **FINITE ELEMENT MODELING OF RC CONNECTIONS STRENGTHENED WITH FRP LAMINATES.** Iranian Journal of Science and Technology, Transaction B, Engineering, Vol. 30, pg 21-30..

12. Carlos A. Coronado and Maria M. Lopez (2006). **SENSITIVITY ANALYSIS OF REINFORCED CONCRETE BEAMS STRENGTHENED WITH FRP LAMINATES.** Journal of Cement and Concrete Composites, Vol 28, pg 102-114.

13. Faustino Sanches Ju´nior, Wilson Sergio Venturini (2007). **DAMAGE MODELING OF REINFORCED CONCRETE BEAMS.** Journal of Advance in Engineering Software, Vol 38, pg 538-546.

14. Omrane Benjeddou, Mongi Ben Ouezdou and Aouicha Bedday (2007). **DAMAGED RC BEAMS REPAIRED BY BONDING OF CFRP LAMINATES.** Journal of Construction and Building Materials, Vol 21, pg 1301-1310.

15. Domenico Bruno, Rodolfo Carpino, Fabrizio Greco (2007). **MODELING OF MIXED MODE DEBONDING IN EXTERNALLY FRP REINFORCED BEAMS.** Journal of Composites Science and Technology, Vol 67, pg 1459-1474.

16. Ayman S. Mosallam, Swagata Banerjee (2007). **SHEAR ENHANCEMENT OF REINFORCED CONCRETE BEAMSSTRENGTHENED WITH FRP COMPOSITES LAMINATES.** Journal of Composites: Part B, Vol 38, pg 781-793.

17. Guido Camata, Enrico Spacone, Roko Zarnic (2007). **EXPERIMENTAL AND NON LINEAR FINITE ELEMENT STUDIES OF RC BEAMS STRENGTHENED WITH FRP PLATES.** Journal of Composites: Part B, Vol 38, pg 277-288.

18. Mohammad Reza Aram, Christoph Czaderski and Masoud Motavalli (2007). **DEBONDING FAILURE MODES OF FLEXURAL FRP STRENGTHENED RC BEAMS.** Journal of Composites: part B, Vol 39, pg 826-841.

19. Ankush Goyal (2007) Structural health monitoring of the retrofitted RC beams using vibrational measurements.

20. N. Pannirselvam, P.N. Raghunath and K.Suguna (2008). **Strength Modelling of Reinforced Concrete Beam with Externally Bonded Fibre Reinforcement Polymer Reinforcement.** American Journal of Engineering and Applied Sciences, Vol 1(3), pg 192-199.

21. T. Zhelyazov, J. Assih, D. Dontchev, A. Li (2008). **Numerical study of the non-linear behaviour of RC beam strengthened by composite materials.** XXVI Rencontres Universitaires de Génie Civil. Nancy, pg 1-8.

22. M.Barbato (2009) **Efficient finite element modelling of reinforced concrete beams retrofitted with fibre reinforced polymers.** Journal of Computers and Structures, Vol 87, pg 167-176.

23. ATENA theory manual part 1 from Vladimir Cervenka, Libor Jendele and Jan Cervenka.